with or integral to plasma membrane (mERs), thereby activating signaling cascades distinct from those of nERs (Beyer et al., 2003; Kelly and Levin, 2001; Segars and Driggers, 2002). We previously reported that pretreatment with estrogens increased neuronal sensitivity to L-glutamate (L-glu) specifically in CA3 in organotypic hippocampal slice cultures. In the same study we found that these effects were mediated by the mechanisms that did not involve nERs (Sato et al., 2002). These results raised the possibility that estrogens affect synaptic contacts in CA3. In the present study, we therefore investigated the effects of E2 on synaptogenesis in the hippocampus and explored the underlying mechanisms using 2 experimental systems. Firstly, we investigated the effects of E2 on the expression of PSD95, a postsynaptic marker, and the spine density in cultured hippocampal slices. Secondly, we investigated the effects of E2 on the number of presynaptic release sites in subregional hippocampal neuron cultures, which were comprised of Ammon's horn neurons, DG neurons, or a mixture of these neurons. It has been reported that in the hippocampus the highest concentration of BDNF occurs in DG granule cells, especially in their axons, mossy fibers (Dieni and Rees, 2002; Scharfman et al., 2003), from the prenatal period through to adulthood (Dieni and Rees, 2002). Although BDNF is known to promote synaptogenesis (Aguado et al., 2003; Alsina et al., 2001; Seil and Drake-Baumann, 2000), it has not been elucidated whether the BDNF in DG granule cells has a role in hippocampal synapse formation. For this reason, we also investigated the relationship between endogenous BDNF in DG granule cells and the effects of E2 in CA3. We here provide evidence showing that E2 induces synaptogenesis between mossy fibers and CA3 neurons by enhancing BDNF release from DG granule cells in a nER-independent and PKA-dependent manner.

2. Results

2.1. *Effects of E2 on postsynaptic sites in cultured hippocampal slices*

We first examined the effect of E2 on the expression of PSD95 in cultured hippocampal slices immunohistochemically. PSD95 is one of the PDZ (PSD-95-Disks large-zona occludens 1/2) domain-containing proteins (Craven and Bredt, 1998; Garner et al., 2000) and is an integral protein of the postsynaptic density. In the control group, the fluorescent signals for PSD95 were apparent in the major hippocampal synaptic sites, i.e., stratum radiatum (SR), stratum oriens (SO), SL and the dentate hilar region (Fig. 1A, left). Because in this study slices were cultured after removing entorhinal cortex, we quantified the expression of PSD95 in CA1SR, CA1SO, CA3SL, and CA3SO, the synaptic sites which maintain the intact presynaptic and postsynaptic cells. Because CA1SR, CA1SO, CA3SL, and CA3SO appeared as fluorescent compartments (Figs. 1B, a and b) in magnified gray-scale mode images, we regarded the averaged fluorescence intensity of each compartment (an outlined area) as the expression level of PSD95 of each synaptic site (see Experimental procedures). When we compared the effects of E2 on the PSD95 expression in CA1 and CA3, E2 (24 h) increased the expression of PSD95 dose-dependently in CA3SL and the effects were significant at 100 nM and the higher concentration (Figs. 1A middle and B). Although E2 also increased the PSD 95 expression in CA3SO at 1 μM (145±9.75% of control), the effect was weaker than that in CA3SL (180±10.2% of control at 1 μM). The distribution pattern of PSD95 signals (including area) in each region was not affected by E2. We then investigated the effect of E2 on the spine density in CA3SL using 1,1′-dioctadecyl-3,3,3′,3′-tetramethylindocarbocyanine perchlorate (DiI) staining. E2 (1 μM, 24 h) markedly increased the spine density at the proximal site of CA3 apical dendrites in CA3SL (296±24.3% of control; Figs. 2A and B). E2 also increased the spine density at the proximal site of CA1 apical dendrites in CA1SR (132±4.49% of control), although to a much lesser extent than that in CA3SL (Fig. 2A). Fig. 2B shows typical images of the proximal sites of CA3 apical dendrites in the control slice (left) and in the E2-treated slice (right). When we immunostained the E2-treated slices with anti-PSD95 antibody after DiI staining, most PSD95 signals in CA3SL clustered on the spine heads (Fig. 2B, right). These results indicate that E2 increased the number of postsynaptic sites in CA3SL. CA3SL is the region in which mossy fibers (DG granule cell axons) make synapses with CA3 pyramidal neurons. We then investigated the effect of E2 on the expression of PSD95 and the spine density in CA3 in DG (–) slices, i.e., the slices of which DG had been excised at 1 DIV. As shown by

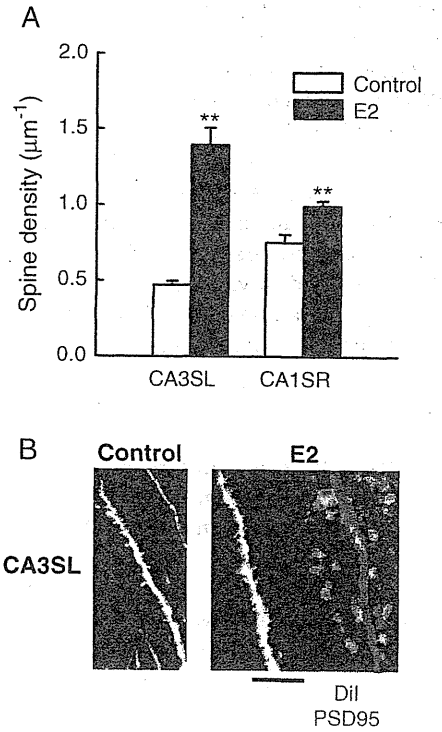

Fig. 2 – Effects of E2 on the spine density in cultured hippocampal slices. (A) E2 (1 μM, 24 h) markedly increased the spine density in CA3SL. **: $p<0.01$ vs. the vehicle control group in each region. $N=8$, Student's t test. (B) Typical images of the DiI-labeled CA3 apical dendrites in the control slice (left) and the E2-treated slice (right). Double staining with DiI and anti-PSD95 antibody revealed that in the E2-treated slice most PSD95 signals (green) were clustered on the spine-heads of the CA3 apical dendrites (red). Bar=5 μm.

Nissl staining, the viability of CA3 pyramidal neurons was not altered by the dissection of the DG (Fig. 3A). The distribution pattern of the PSD95 signals was not affected, either (Fig. 3B). E2 (1 μM, 24 h) affected neither the expression level (Fig. 3C) nor the distribution pattern of PSD95 in DG (–) slices (data not shown). The effect of E2 (1 μM, 24 h) on the spine density in CA3SL was also abolished in DG (–) slices (Fig. 3D). Taken together, these results suggest that E2 induces synaptogenesis between mossy fibers and CA3 pyramidal neurons.

2.2. *Effects of E2 on presynaptic sites in subregional hippocampal neuron cultures*

We next investigated the effect of E2 on the number of presynaptic sites using subregional hippocampal neuron cultures, which were comprised of Ammon's horn neurons, DG neurons, or a mixture of these neurons, respectively. We quantified the number of presynaptic sites by counting the number of sites in which depolarization-induced uptake and release of (N-(3-triethylammoniumpropyl)-4-(4-(dibutylamino)styryl)pyridinium dibromide (FM1-43) (Cochilla et al., 1999) had occurred (see Experimental procedures). Fig. 4A shows the typical morphologies of neurons in the Ammon's horn neuron culture (left) and in the DG neuron culture (middle). Most cells in the Ammon's horn neuron culture were large and spindle-shaped, whereas most cells in the DG neuron culture were small and granular. As shown in Fig. 4B, E2 (1 μM, 24 h) significantly increased the number of presynaptic sites in the mixed neuron culture (199±9.18% of control). E2 also increased the number of presynaptic sites in the DG neuron culture (170±12.1% of control), but not in the Ammon's horn neuron culture. Fig. 4C shows the typical fluorescent images of presynaptic sites (red puncta) in the control group (top left) and in the E2-treated group (top right) in the mixed neuron culture. We confirmed that E2 had no effect on the number of surviving neurons in each culture by immunostaining with anti-NeuN antibody (data not shown). These results indicate that E2 increased the number of presynaptic sites in the hippocampal neuron cultures and that DG neurons are indispensable for this effect.

2.3. *The effects of E2 in hippocampal slice cultures and subregional hippocampal neuron cultures were mediated by the mechanism which is independent of nERs and dependent on endogenous BDNF*

Pharmacological experiments were performed to investigate and compare the mechanisms underlying the effects of E2 in hippocampal slice cultures and subregional hippocampal neuron cultures (the mixed neuron culture) (Fig. 5). First, we examined the contribution of nERs using ICI, a strong antagonist to both of ERα (Ki: 1.5 nM) and ERβ (Ki: 6.4 nM) (Kuiper et al., 1997). ICI at a concentration of 1 μM did not alter the effect of E2 on the expression of PSD95 expression, the spine density, and the number of presynaptic sites (Figs. 5A–C). It has been reported that DG granule cells have the highest concentration of BDNF in the hippocampus, especially in the mossy fibers (Dieni and Rees, 2002; Scharfman et al., 2003). Because BDNF is known to enhance synapse formation (Aguado et al., 2003; Alsina et al., 2001; Seil and Drake-

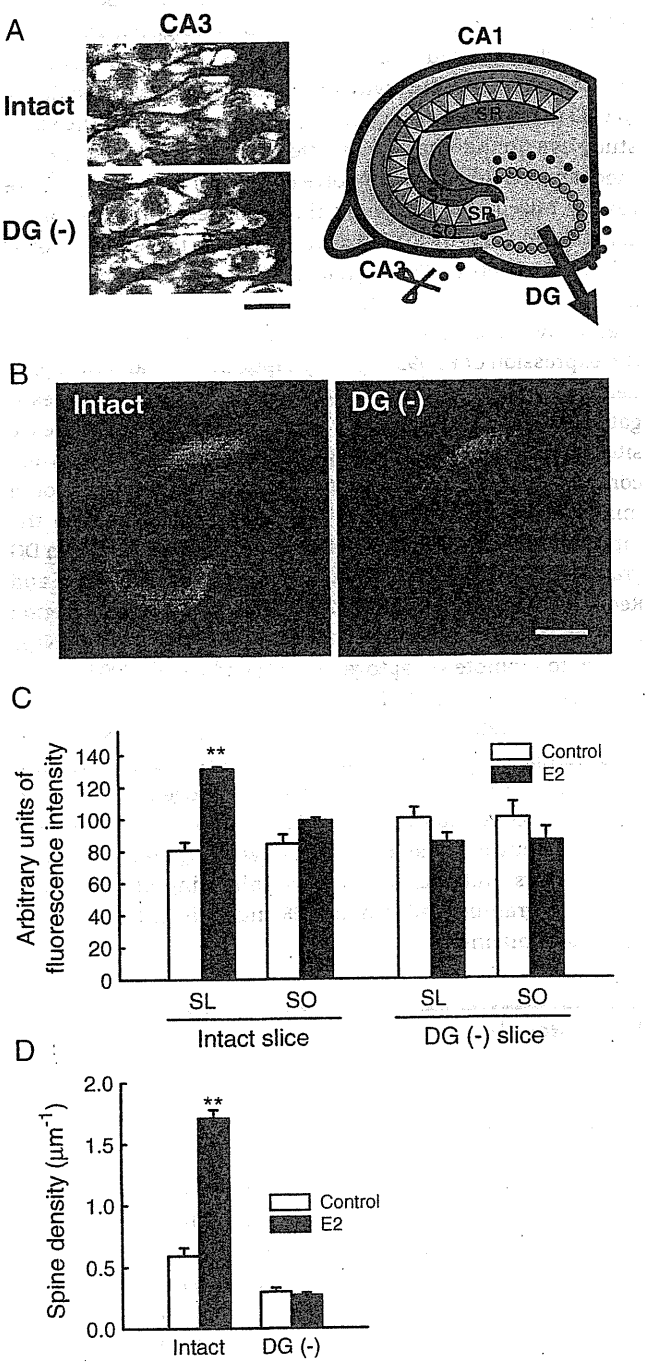

Fig. 3 – Effects of E2 on the expression of PSD95 and the spine density in cultured hippocampal slices of which DG had been excised at 1 DIV. (A) The viability of CA3 pyramidal neurons in DG (–) slices. Nissl staining revealed that their viability was not affected by the dissection of DG. Bar=20 μm. (B) Immunoreactive signals of PSD95 in a DG (–) slice. The distribution pattern of the PSD95 signals was not affected by the dissection of DG. Bar=500 μm. (C) The effect of E2 on the expression of PSD95 in DG (–) slices. E2 (1 μM, 24 h) did not affect the expression of PSD95 in CA3 in DG (–) slices. (D) The effect of E2 on the spine density in CA3SL in DG (–) slices. E2 (1 μM, 24 h) did not affect the spine density in CA3SL in DG (–) slices.

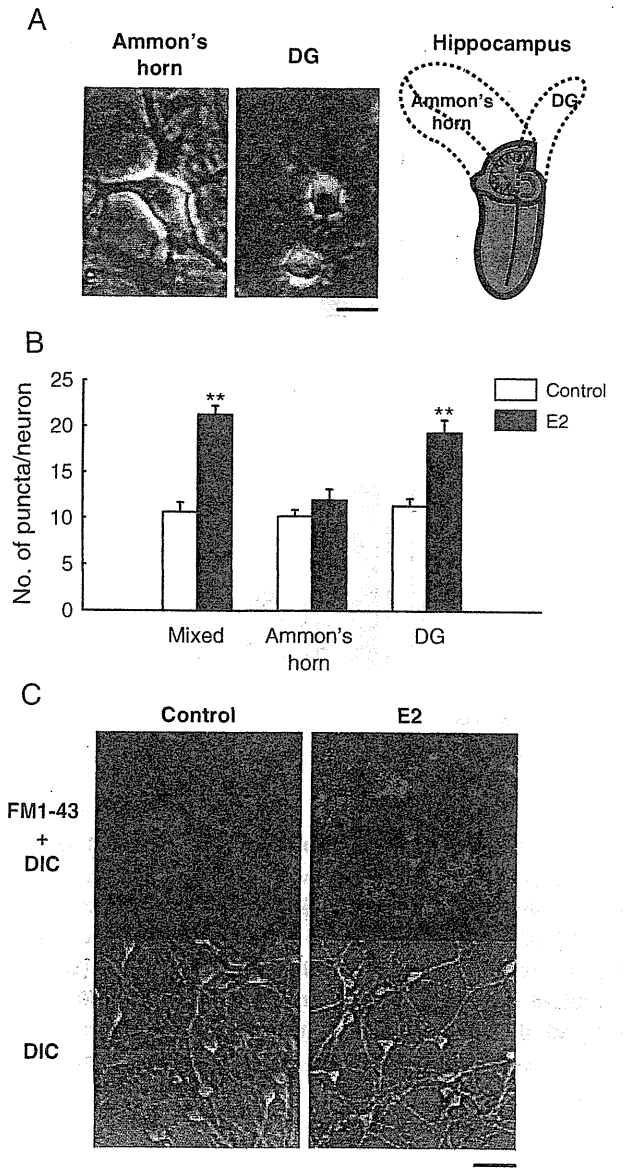

Fig. 4 – Effects of E2 on the number of presynaptic sites in subregional hippocampal neuron cultures. (A) Typical cell morphologies in the Ammon's horn neuron culture (left) and in the DG neuron culture (middle). Bar=20 μm. (B) E2 (1 μM, 24 h) significantly increased the number of presynaptic sites in the mixed neuron culture and in the DG neuron culture. **: $p<0.01$ vs. the control group in each culture. $N=8$, Student's t test. (C) Typical images of presynaptic sites visualized by FM1-43 (red puncta) in the control group (top left) and in the E2-treated group (top right) in the mixed neuron culture. DIC images of the same microscopic views were also shown (bottom left and bottom right). Bar=50 μm.

Baumann, 2000), we examined the involvement of BDNF in the effects of E2. K252a (200 nM), a potent inhibitor of the high affinity receptor of BDNF (TrkB) (Squinto et al., 1991; Bothwell, 1995), significantly inhibited the effects of E2 on the expression of PSD95 expression, the spine density, and the number of presynaptic sites (Figs. 5A–C). Furthermore BDNFAB (10 μg/ml) significantly inhibited the effects of E2 in these experiments (Figs. 5A–C). These inhibitors alone had no effects in each case. These results indicate that the effects of E2 in hippocampal

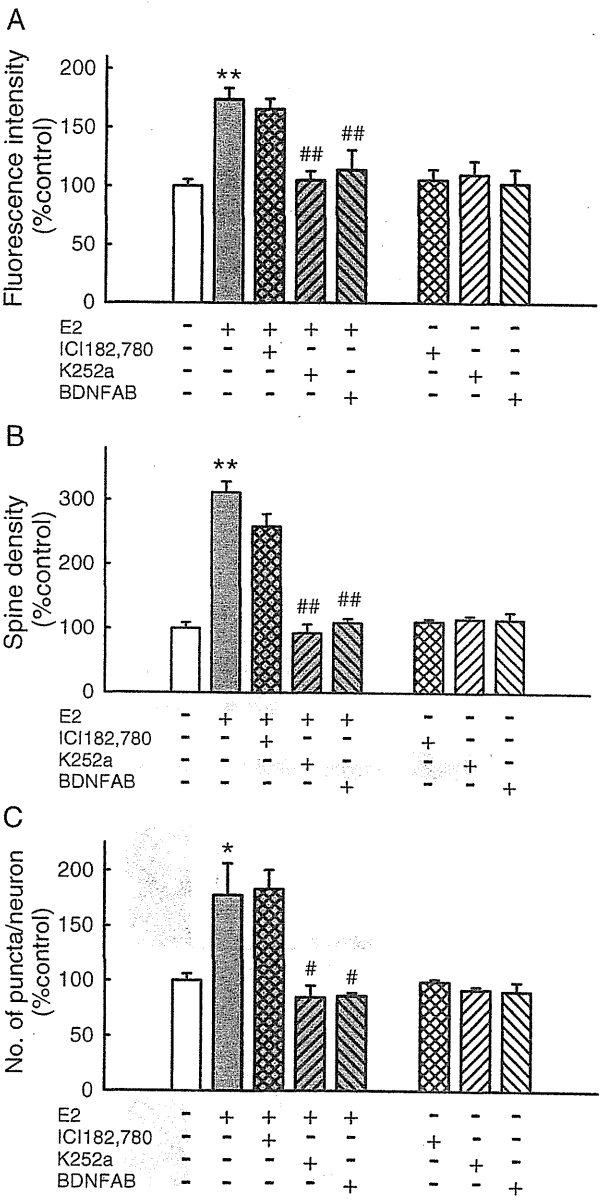

Fig. 5 – Effects of ICI, K252a, and BDNFAB on the effects of E2 in hippocampal slice cultures and subregional hippocampal neuron cultures. (A) K252a (200 nM) and BDNFAB (10 μg/ml) significantly inhibited the effect of E2 on the expression of PSD95 in cultured hippocampal slices, whereas ICI (1 μM) did not. **: $p<0.01$ vs. the control group, ##: $p<0.01$ vs. the E2-treated group. $N=8$, Tukey's test following ANOVA. (B) K252a (200 nM) and BDNFAB (10 μg/ml) significantly inhibited the effect of E2 on the spine density in cultured hippocampal slices, whereas ICI (1 μM) did not. **: $p<0.01$ vs. the control group, ##: $p<0.01$ vs. the E2-treated group. $N=8$, Tukey's test following ANOVA. (C) K252a (200 nM) and BDNFAB (10 μg/ml) significantly inhibited the effect of E2 on the number of presynaptic sites in the mixed neuron culture, whereas ICI (1 μM) did not. *: $p<0.05$ vs. the control group, #: $p<0.05$ vs. the E2-treated group. $N=8$, Tukey's test following ANOVA.

slice cultures and subregional neuron cultures were mediated by the common mechanism which is independent of nERs and dependent on endogenous BDNF, suggesting the involvement of BDNF in DG granule cells in the synaptogenic effect of E2 in CA3SL.

2.4. *E2 enhanced BDNF release from DG granule cells via nER-independent and PKA-dependent mechanisms*

We further examined the association between the effects of E2 and BDNF using subregional hippocampal neuron cultures. The expression levels of BDNF were confirmed for both the Ammon's horn neuron culture and the DG neuron culture by Western blot analysis and enzyme linked immunosorbent assay (ELISA) (Fig. 6). In Western blot analysis, BDNF immunoreactive bands were detected in the control lanes for both cultures, but the OD for the DG neurons was markedly higher than that for the Ammon's horn neurons (Fig. 6A). E2 (1 μM, 24 h) did not affect the expression levels of BNDF in Ammon's horn neurons or DG neurons. ELISA also showed that the expression level of BDNF in DG neurons was remarkably higher than that of Ammon's horn neurons and E2 had no effect on the expression levels in both cultures (Fig. 6B). These results indicate that subregional neuron cultures reflect in vivo pattern of BDNF expression in the hippocampus, in which the highest concentration of BDNF occurs in DG granule cells (Dieni and Rees, 2002; Scharfman et al., 2003). We next examined the possibility that E2 enhances BDNF release from DG granule cells without affecting BDNF expression. The amount of BDNF released into the culture medium of the DG neuron culture was measured by ELISA. We performed ELISA after 10 h of treatment with E2, at the time point when the effect of E2 on the number of presynaptic sites was not yet apparent (Fig. 7A). E2 (1 μM, 10 h) remarkably increased the BDNF release (267 ± 20.5% of control; Fig. 7B). Neither ICI (1 μM) nor U0126 (10 μM) (Ki: 72 nM for MEK1, 58 nM for MEK2) (Duncia et al., 1998), influenced the effect of E2. In contrast, KT5720 (200 nM) (Ki: 56 nM for PKA) (Kase et al., 1987) and Rp-cAMP (10 μM) (Ki: 11 μM for PKA) (Rothermel and Parker Botelho, 1988), suppressed the effect of E2 to the control level. These inhibitors alone had no effects on the basal BDNF release. These results indicate that E2 enhanced BDNF release from DG

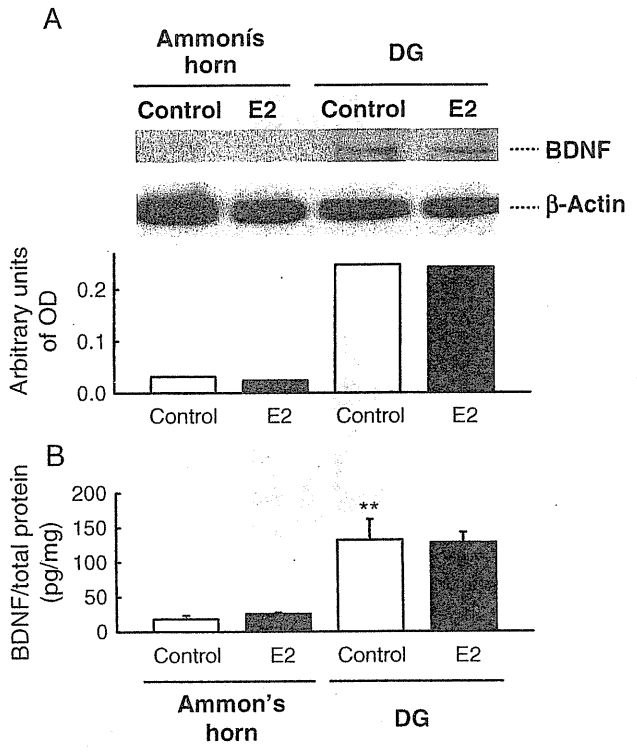

Fig. 6 – The expression of BDNF in subregional hippocampal neuron cultures. (A) Western blot analysis of BDNF in subregional hippocampal neuron cultures. The expression level of BDNF of DG neurons was much higher than that of Ammon's horn neurons. E2 (1 μM, 24 h) had no effect on the BDNF expression level. The same results were obtained in 3 independent experiments. (B) ELISA detection of BDNF in subregional hippocampal neuron cultures. The expression level of BDNF in DG neurons was significantly higher than that in Ammon's horn neurons. E2 (1 μM, 24 h) had no effect on the BDNF expression level. **: $p<0.01$ vs. the control group of Ammon's horn neurons. $N=4$, Tukey's test following ANOVA.

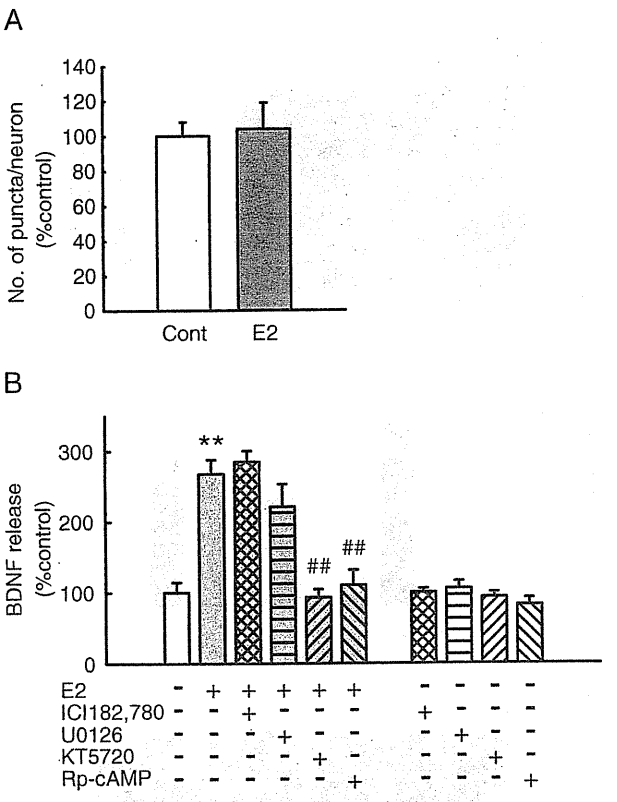

Fig. 7 – Effects of E2 on the BDNF release in the DG neuron culture. (A) Treatment for 10 h with E2 (1 μM) had no effect on the number of presynaptic sites in the DG neuron culture. (B) E2 (1 μM, 10 h) significantly enhanced BDNF release in the DG neuron culture. KT5720 (200 nM) and Rp-cAMP (10 μM) inhibited the effect of E2, whereas ICI (1 μM) and U0126 (10 μM) did not. **: $p<0.01$ vs. the control group, ##: $p<0.01$ vs. the E2-treated group. $N=4$, Tukey's test following ANOVA.

granule cells via nER-independent and PKA-dependent mechanisms, which may underlie the effects of E2 described above.

3. Discussion

In this study, we provided evidence showing that E2 induces synaptogenesis between mossy fibers and CA3 neurons by enhancing BDNF release from DG granule cells in a nER-independent and PKA-dependent manner.

We used subregional hippocampal neuron cultures to investigate the effects of E2 in detail. That these cultures sufficiently maintain their region-specific characters is supported by the following evidence: 1) the morphology of neurons in the Ammon's horn neuron culture was clearly different from that in the DG neuron culture (Fig. 4A). Most cells in the Ammon's horn neuron culture were large and spindle-shaped, which is typical for pyramidal neurons. Most cells in the DG neuron culture were small and granular, which is typical for DG granule cells. 2) DG neurons isolated and cultured using a similar procedure maintain their in vivo physiological properties (Ikegaya et al., 2000). 3) The expression level of BDNF of the cultured DG neurons is much higher than that of the cultured Ammon's horn neurons, reflecting in vivo pattern of BDNF expression in the hippocampus, in which the highest concentration of BDNF occurs in DG granule cells (Dieni and Rees, 2002; Scharfman et al., 2003).

In our study, we prepared hippocampal slices from both genders of P8 rat pups and cultured for 10 days with medium supplemented with horse serum (HS) collected from gelding horses, in which steroid concentrations were under the limits for detection. Because the increases in the expression level of PSD95 and the spine density in CA3 were observed in all slices treated with E2, we consider that the effects of E2 in our study are gender-independent. Currently we are investigating whether or not there is gender difference in the extents of the effects of E2. Organotypic hippocampal slice cultures of P5–9 rat brains are well-established, stable model for investigating hippocampal function including developmental synaptogenesis because neurons maintain synaptogenic ability in each region (CA1, CA3, and DG) (De Simoni et al., 2003; Mizuhashi et al., 2001; Qin et al., 2001). It has been reported that during postnatal development, the capacity of estrogen binding protein is high enough to lower the concentrations of serum estrogens to nonphysiological levels (Germain et al., 1978). This suggests that the conditions for the hippocampal slice culture in the present study more closely represent the postnatal developmental stage. Recently it was clarified that E2 is synthesized from endogenous cholesterol by P45017α and P450 aromatase in hippocampal neurons (Hojo et al., 2004) and that it plays an essential role in the maintenance of synapses (Kretz et al., 2004). The effects of E2 shown here might be achieved by locally synthesized E2 at the postnatal developmental stage. Two previous studies reported the effects of E2 on spinogenesis in cultured hippocampal slices (Kretz et al., 2004; Pozzo-Miller et al., 1999), but their results are conflicting, perhaps because of the effects of various steroids included in the HS in the culture medium.

Our findings suggest that BDNF in DG granule cells mediates the effects of E2. It has been reported that in the hippocampus the highest concentration of BDNF occurs in DG granule cells, especially in their axons, mossy fibers (Dieni and Rees, 2002; Scharfman et al., 2003), from the prenatal period through to adulthood (Dieni and Rees, 2002). The significance of BDNF in DG granule cells, however, had been unknown until Scharfman et al. showed that endogenous BDNF in mossy fibers affected the excitability of CA3 neurons in adult female rats (Scharfman et al., 2003). On the other hand, BDNF has long been known to promote synaptogenesis by maturation of presynaptic sites (Aguado et al., 2003; Seil and Drake-Baumann, 2000). Real-time monitoring revealed that BDNF increases the number of presynaptic sites (Alsina et al., 2001). Presynaptic maturation can induce postsynaptic maturation, as shown by mossy fiber induction of postsynaptic maturation including assembly and clustering of PSD95 on CA3 apical dendrites (Qin et al., 2001). In the present study, BDNF released from DG granule cells may have first increased the number of presynaptic sites by autocrine/paracrine mechanisms, thereby inducing the maturation of postsynaptic sites. In addition to the communication with CA3 pyramidal neurons through giant boutons, mossy fibers also communicate with local circuit interneurons in CA3 through filopodial extensions and en passant boutons (Acsady et al., 1998; Lawrence and McBain, 2003). Although the number of these small terminals is greater than that of giant boutons, we consider that E2 predominantly promoted the synaptogenesis between mossy fibers and CA3 pyramidal neurons in this study because of the following reasons: 1) E2 increased the number of giant boutons, which were identified as mossy fiber terminals containing Zn^{2+} in our previous report (Sato et al., 2002), and 2) the major population of BDNF-positive mossy fiber terminals is those with giant boutons (Danzer and McNamara, 2004). Further experiments using interneuron-specific markers will be necessary to identify the effect of E2 on synaptogenesis between mossy fibers and CA3 interneurons.

E2 enhanced BDNF release from DG granule cells in a nER-independent and PKA-dependent manner. Besides the genomic effects via nERs (ERα and ERβ), recent reports have described the nongenomic effects of estrogens mediated by mERs (Beyer et al., 2003; Kelly and Levin, 2001; Segars and Driggers, 2002). Although the membrane localization of the E2 binding sites is widely accepted, mERs still await isolation and gene cloning. One of the candidate mERs is membrane-localized ERα/β that can activate signal transduction pathways distinct from nERα/β (Razandi et al., 2004; Thomas et al., 2004). Although the mode of action has not been elucidated precisely, ERα has been localized to the neuronal plasma membrane in the hippocampus (Clarke et al., 2000). On the other hand, several reports suggest that the proteins, which are completely different from ERα/β, function as mERs in hypothalamus (Cambiasso and Carrer, 2001), midbrain (Beyer and Karolczak, 2000; Beyer et al., 2002), and neocortex (Toran-Allerand et al., 2002). The effects of E2 observed in our study may have been mediated by one or more mechanisms other than nERs.

It has been reported that E2 modulates the expression of BDNF by genomic (Sohrabji et al., 1995) or nongenomic mechanisms (Ivanova et al., 2001). Unexpectedly, in this

study BDNF expression levels were not affected by E2 (Fig. 6). Instead, E2 enhanced BDNF release from DG granule cells via the activation of the PKA pathway. The PKA/cAMP-responsive element binding protein (CREB) pathway has been shown to lie downstream of mERs in midbrain dopamine neurons (Beyer and Karolczak, 2000; Beyer et al., 2002). The effects of E2 in this study might be mediated by the same type of mERs as those in midbrain dopamine neurons. There are 2 major BDNF secretory pathways (for review, Lessmann et al., 2003): one is the Ca^{2+}-independent constitutive pathway and the other is the Ca^{2+}-dependent regulated pathway. In the regulated pathway, BDNF is sorted to large dense-core vesicles (LDCVs) (Wu et al., 2004) and released in an activity-dependent manner (Haubensak et al., 1998) following slow kinetics typical for protein secretion (Hartmann et al., 2001). BDNF plays an important role in long-term synaptic plasticity (for review, McAllister et al., 1999). BDNF is released selectively by electrical stimulation patterns that induce long-term-potentiation (LTP), thereby modulating the activity-dependent neuronal plasticity (Balkowiec and Katz, 2002; Gartner and Staiger, 2002). cAMP triggers BDNF release in such LTP-inducing condition (Patterson et al., 2001), so E2 might affect synaptic plasticity by way of cAMP-dependent BDNF release.

In ovariectomized adult female rats, E2 enhances the spinogenesis of apical dendrites in CA1 but not in CA3 (Gould et al., 1990). Recent studies have revealed that Akt (protein kinase B) activation via mERs mediates the spinogenesis in CA1 in adult rats (McEwen et al., 2001; Znamensky et al., 2003). On the other hand, there is evidence for another mechanism of E2-induced spinogenesis in embryonic hippocampal neuron cultures. In this system E2 acts via nERs to suppress BDNF expression in γ-aminobutyric acid (GABA) ergic interneurons and to decrease GABAergic inhibition, thereby inducing spinogenesis (Murphy et al., 1998a; Murphy et al., 1998b). It is possible that these mechanisms were also active in our study because E2 increased the spine density in CA1SR in cultured hippocampal slices. But clear differences were observed between the effect in CA1SR and that in CA3SL. The spinogenic effect in CA1SR was much weaker than that in CA3SL (Fig. 2) and the expression of PSD95 in CA1SR was not changed by E2 (Fig. 1). The local assembly of PSD95 is spatially and temporally correlated with the maturation of spine morphogenesis (Okabe et al., 2001: Jontes and Smith, 2000). PSD95 clusters are found in one-half of dendritic filopodia, but in most mature spines (Takahashi et al., 2003). Thus, the spines induced by E2 in CA1SR may be more immature compared with those in CA3SL. The effects of E2 in CA3 through BDNF derived from DG granule cells may be stronger than that in CA1 through the mechanisms described above. The absence of the effect of E2 in CA3 in previous reports (Gould et al., 1990; Znamensky et al., 2003) can be explained if the mechanism that we indicated here is not active in adulthood or the mechanisms demonstrated in the previous reports are active predominantly in CA1.

Our results strongly suggest that E2 induces synaptogenesis between mossy fibers and CA3 neurons by the enhancement of BDNF release from DG granule cells in a nER-independent and PKA-dependent manner. These data provide evidence that BDNF in DG granule cells has a role in synaptogenesis, and that E2 can modulate this synaptogenic function of BDNF.

4. Experimental procedure

4.1. Materials

Millicell-CM was from Millipore (Bedford, MA). Minimal essential medium (MEM), Neurobasal medium (NB) and B-27 supplement were from Gibco Invitrogen Co. (Carlsbad, CA). Donor HS (gelding) was from C-C Biotech Corporation (Valley Center, CA). Paraformaldehyde (PFA), polyoxyethylene (10) octylphenyl ether (Triton X-100), ammonium chloride, dimethylsufoxide (DMSO), L-glutamine, glycine, Tween 20 and sodium azide were from Wako Pure Chemical (Osaka, Japan). K252a was from Calbiochem (Darmstadt, Germany). Anti-BDNF antibodies (AB1534SP and AB1513P) and Chemikine BDNF Sandwich ELISA kit were from Chemicon (Temecula, CA). ICI was from Tocris (Ballwin, MO). Mouse monoclonal immunoglobulin G (IgG) to PSD95 (K28/43) was from Upstate Biotechnology (Lake Placid, NY). Alexa Fluor 488 rabbit anti-mouse IgG, NeuroTrace fluorescent Nissl, DiI and FM1-43 were from Molecular Probes (Eugene, OR). E2, poly-L-lysine, cytosine β-D-arabino-furanoside (AraC), ethylenediaminetetraacetic acid (EDTA), phenylmethylsulphonyl fluoride, leupeptin, antipain hydrochloride, aprotinin, Trizma hydrochloride, bovine serum albumin (BSA), rabbit polyclonal IgG to β-actin, peroxidase-conjugated anti-rabbit IgG, tetrodotoxin (TTX), KT5720, and Rp-cAMP were from Sigma (St. Louis, MO). U0126 was from Promega (Madison, WI). Sodium dodecyl sulphate (SDS) was from Nacalai tesque (Kyoto, Japan). ADVASEP-7 was from Biotium (Hayward, CA). Enhanced chemiluminescence (ECL) plus Western blotting detection kit was from Amersham Biosciences (Arlington Heights, IL). Fluorescent images were obtained using a BioRad μ-Radiance laser scanning confocal system (Hercules, CA) attached to Nikon inverted microscope (Tokyo, Japan). Image analysis was performed using Adobe Photoshop 7.0 (Mountain View, CA).

4.2. Organotypic hippocampal slice culture

All animal procedures were in accordance with the guidelines of the National Institute of Health Sciences, Japan, to minimize pain or discomfort. Organotypic slice cultures of both genders of P8 Wistar rat hippocampi were prepared according to the method of Sato et al. (2002). Briefly, horizontal medial hippocampal slices (300-μm thick) were placed on Millicell-CM transmembranes and cultured with 0.7 ml of the culture media (50% [vol/vol] MEM, 25% [vol/vol] Hank's balanced salt solution [HBSS], and 25% [vol/vol] HS [gelding] supplemented with 6.5 mg/ml glucose, 50 U/ml penicillin G potassium and 100 μg/ml streptomycin sulphate). All experiments were performed at 10 days in vitro (DIV) because cultured hippocampal slices recover from damage by sectioning and complete the trisynaptic neuronal circuitry (DG→CA3→CA1) at 10–14 DIV (Nakagami et al., 1997).

4.3. Immunohistochemistry

Immunostaining of cultured hippocampal slices was performed according to the method of Qin et al. (2001) with modifications. Slices were fixed with ice-cold 4% (wt/vol) PFA in 0.1 M phosphate buffer (PB) for 10 min at 4 °C, washed with phosphate buffered saline (PBS) (5 min×3), and treated with 1% (vol/vol) Triton X-100 in PBS overnight at 4 °C. Slices were then blocked with 50 mM ammonium chloride for 30 min at 4 °C and 20% HS in PBS for 30 min at 4 °C. Subsequent steps were carried out using PBS containing 1% HS. Slices were treated with mouse monoclonal IgG to PSD95 (1:1000) overnight at 4 °C, washed (15 min×3), and treated with Alexa Fluor 488 rabbit anti-mouse IgG (1:1000) overnight at 4 °C. After washing (15 min×3), fluorescent images were obtained by confocal microscopy (BioRad μ-Radiance laser scanning confocal system) using a 4×objective. Black level was set so that the averaged fluorescence intensity of 5 independent squares (20 μm×20 μm) placed at the medial position of CA1 stratum pyramidale (SP) of the control slice had the same value as that of the outside of the slice. Gain level was set so that the averaged fluorescence intensity of 5 squares (20 μm×20 μm) placed at the medial position of CA3SL of the control slice was at the half-maximum level. In gray-scale mode under these settings, the major synaptic sites appeared as fluorescent compartments as shown in Fig. 1B. When we outlined these compartments as indicated in Fig. 1B and calculated the areas, the values were constant regardless of the treatment (data not shown), so, we measured the averaged fluorescence intensity of each compartment (an outlined area) and subtracted the back ground intensity to quantify the expression level of PSD95 of each synaptic site. Because slices were cultured after removing entorhinal cortex, we quantified the expression of PSD95 in CA1SR, CA1SO, CA3SL, and CA3SO, the synaptic sites which maintain the intact presynaptic and postsynaptic cells (Fig. 1B).

4.4. DiI staining

Cultured hippocampal slices were fixed with 4% PFA for 30 min at 4 °C. The fixative above the transmembrane was removed and DiI crystals were embedded into CA1SO and CA3SO under the light microscope. After 3 days of incubation at 4 °C, fluorescent images were obtained by confocal microscopy using a 60×objective. Horizontal optical sections were taken at 0.5 μm steps and the resultant z-series images were summed into a flat image. Spines (both dendritic filopodia and mature spines) were counted at the proximal sites of apical dendrites projecting from pyramidal cell bodies. For double labeling with DiI and PSD95 immunostaining, slices were immunostained after 3 days of incubation with DiI crystals.

4.5. Fluorescent Nissl staining

Cultured hippocampal slices were fixed with 4% PFA for 60 min at 4 °C. Subsequent steps were carried out at room temperature. After washing with PBS (15 min×3), the slices were treated with 0.1% Triton X-100 in PBS for 60 min, washed with PBS for 10 min, and incubated with NeuroTrace fluorescent Nissl (1:30 in PBS) for 40 min in a dark room. The incubation was terminated by a 10 min wash with 0.1% Triton X-100 in PBS, followed by 2 h wash with PBS. Fluorescent images were obtained by confocal microscopy using a 60×objective.

4.6. Subregional hippocampal neuron culture

Subregional neuron cultures of both genders of P3 Wistar rat hippocampi were prepared according to the method of Ikegaya et al. (2000). Ammon's horn and DG were isolated from hippocampi with extreme care so as not to mix these 2 regions (Fig. 4A, right). Dissociated cells from Ammon's horn, DG, or a combination of these regions were suspended in a 1:1 mixture of astrocyte-conditioned medium (ACM) and NB/B27 medium (2% [v/v] B-27 supplement and 73 μg/ml L-glutamine in NB) and plated onto 48-well plates coated with poly-L-lysine. After 24 h, the medium was changed to ACM-free NB/B-27 medium containing 2 μM AraC. Cells derived from each region were cultured for 7 days at the same cell density (2×10^4 cells/cm^2 for FM1-43 analysis, 5×10^5 cells/cm^2 for Western blot analysis and ELISA detection of BDNF). All surviving cells were immunohistochemically confirmed to be neurons using anti-NeuN antibody (data not shown).

4.7. FM1-43 analysis

After 1 h of incubation with HBSS at 37 °C, cultured neurons were treated with 10 μM FM1-43, a styryl pyridinium dye (Cochilla et al., 1999) in high K^+-HBSS (20 mM KCl; osmolarity maintained by concomitant decrease in sodium concentration) for 2 min and washed gently with HBSS for 1 min. To reduce background staining, neurons were washed with 20 μM ADVASEP-7, a sulphobutylated derivative of β-cyclodextrin (Tait et al., 1992) for 1 min. ADVASEP-7 has a higher affinity for FM1-43 than plasma membranes and has been shown to greatly reduce background staining in brain slices (Kay et al., 1999). After the incubation with 10 μM TTX for 30 min, three images ([1] stained image; [2] destained image obtained after the treatment with high K^+-HBSS; and [3] differential interference contrast [DIC] image) were obtained for each microscopic field of view using confocal microscopy with a 10× objective. The second image was subtracted from the first, which revealed the presynaptic sites where depolarization-specific release had occurred (Fig. 4C, top panels). The fluorescent puncta in each microscopic field of view were counted. The number of synapses per neuron was estimated by dividing the total number of puncta by the number of neurons observed in the third (DIC) image (Fig. 4C, bottom panels).

4.8. Western blot analysis

Cultured neurons were washed twice with ice-cold PBS and then harvested on ice with 50 mM Tris buffer (pH 7.2) containing 1 mM EDTA, 1 mM phenylmethylsulphonyl fluoride, 1 mM leupeptin, 1 μg/ml antipain and 1 μg/ml aprotinin. After intense sonication (23 kHz, 1 min×3), the cell suspension was centrifuged at 800×g for 5 min at 4 °C. An

aliquot of this supernatant was removed for the protein assay. Another aliquot was diluted in SDS sample buffer. Protein samples containing an equal amount of protein were separated by electrophoresis on 10% polyacrylamide-SDS gels and transferred onto polyvinyliden difluoride membranes in 49.6 mM Tris, 384 mM glycine and 0.01% (wt/vol) SDS at 30 V overnight followed by 80 V for 1 h. The membranes were incubated with Tris-buffered saline (TBS) containing 0.1% (vol/vol) Tween 20, 5% (wt/vol) skim milk, 2% (wt/vol) BSA, and 0.1% (wt/vol) sodium azide for 1 h, followed by overnight incubation with protein A purified rabbit anti-BDNF polyclonal antibody (AB1534SP, Chemicon) (1:1000) or rabbit polyclonal IgG to β-actin (1:1000) at 4 °C. After washing (30 min), the membranes were then incubated with peroxidase-conjugated anti-rabbit IgG (1:1000) for 1 h at room temperature. Immunoreactive bands were visualized using the ECL kit. Optical densities (ODs) of immunoreactive bands were measured based on a gray scale of 0–256 arbitrary units. Background was subtracted from the OD and this corrected value was normalized to the corrected value of the β-actin band obtained from the same sample.

4.9. *ELISA detection of BDNF*

In comparison of BDNF contents in cultured DG neurons and cultured Ammon's horn neurons, cells were washed twice with ice-cold PBS and then harvested on ice with homogenization buffer consisting of 100 mM Trin/HCl (pH7), containing 2% (wt/vol) BSA, 1 M NaCl, 4 mM EDTA.Na2, 2% (vol/vol) Triton X-100, 0.1% (wt/vol) sodium azide, 5 μg/ml aprotinin, 0.5 μg/ml antipain, 157 μg/ml benzamidine, 0.1 μg/ml pepstatin A and 17 μg/ml phenylmethyl–sulphonyl fluoride. After intense sonication (23 kHz, 1 min×3), the homogenates are centrifuged at 14,000×*g* for 30 min. An aliquot of this supernatant was removed for the protein assay. Another aliquot was subjected to the calculation of BDNF concentration by the Chemikine BDNF sandwich ELISA kit. The plates, which were pre-coated with monoclonal antibodies against BDNF, were incubated with 100 μl of supernatant in each well overnight, followed by incubation with the secondary antibody for 3 h and color developing procedures for 1 h. Immediately after the stop solution included in the kit was added, the ODs of 450 nm were measured. A standard curve was run for each plate and linearity was confirmed for all detections. Because the lower detection limit of the kit is 7.8 pg/ml, we used data from the experiments in which the control value was higher than this limit. The concentration of BDNF was normalized to the total amount of protein. In the calculation of BDNF contents in the culture media, the culture media were collected after 10 h of incubation with E2, centrifuged at 1500×*g*, and the concentration of BDNF in the supernatants was determined by ELISA. Because in this case the values of the control group varied from experiment to experiment by several folds, we set 'basal value' in each experiment. 24 h after medium change, BDNF concentrations in the culture media were calculated and averaged for 4 wells in one experiment. This value was taken as the 'basal value' and the data were normalized to this 'basal value' in each experiment.

4.10. *Drug treatment*

E2 was dissolved at 100 mM in ethanol and diluted to the final concentrations with the culture medium. For PSD95 immunohistochemistry and FM1-43 analysis, cultured slices and cells were treated with various concentrations of E2 for 24 h. ICI (Ki: 1.5 nM for ERα, 6.4 nM for ERβ; Kuiper et al., 1997) was dissolved at 1 mM in ethanol and co-applied at 1 μM with E2. K252a (Squinto et al., 1991; Bothwell, 1995) was dissolved at 1 mM in DMSO and co-applied at 200 nM with E2. This concentration completely blocks the effect of BDNF in cultured hippocampal slices (Koyama et al., 2004). BDNFAB (protein A purified sheep anti-BDNF polyclonal antibody, AB1513SP, Chemicon) was dissolved in the culture medium at 10 μg/ml. This concentration blocks the effect of endogenous BDNF (Rasika et al., 1999; Matsunaga et al., 2004). For ELISA detection of the released BDNF, cultured cells were treated with E2 for 10 h. KT5720 (Ki: 56 nM) (Kase et al., 1987) was dissolved in the ethanol at 1 mM and co-applied at 200 nM with E2. Rp-cAMP (Ki: 11 μM) (Rothermel and Parker Botelho, 1988) was dissolved in PBS at 10 mM and co-applied at 10 μM with E2. U0126 (Ki: 72 nM for MEK1, 58 nM for MEK2) (Duncia et al., 1998) was dissolved in DMSO at 10 mM and co-applied at 10 μM with E2. We also confirmed beforehand that 0.1% ethanol or 0.1% DMSO (the maximal concentration used for vehicle in our experiments) alone had no effects in cultured hippocampal slices and subregional hippocampal neuron cultures (Fig. S1).

4.11. *Data analysis*

All data regarding the expression level of PSD95, the spine density, and the number of FM1-43 positive puncta, were quantified in a blinded manner. For quantification of PSD-95 signals, the fluorescence intensities in the synaptic sites were averaged for 4 slices in one experiment. These values were then averaged for 8 independent experiments (separate platings) and statistical analysis was performed using one-way repeated-measure analysis of variance (ANOVA) and the post hoc Tukey's test for multiple pairwise comparisons. Data are shown as the values normalized to that of CA1SR in the control group. The spine densities (the number of spines per μm of dendrite) averaged for 8 to 10 neurons per slice were averaged for 4 slices in 1 experiment. These values were then averaged for 8 independent experiments (separate platings) and statistical analysis was performed using the Student's t test. For FM1-43 analysis, the numbers of presynaptic sites (per neuron) were averaged for 4 wells in 1 experiment. These values were then averaged for 8 independent experiments (separate platings) and statistical analysis was performed using the Student's t test. In multiple pharmacological treatments, data were collected according to the methods described above, and statistical analysis was performed by one-way repeated-measure ANOVA and the post hoc Tukey's test for multiple pairwise comparisons. Data were shown as the values normalized to that of the control group. For ELISA detection of BDNF expression, the normalized values (BDNF/total protein) were averaged for 4 wells in one experiment. These values were then averaged for 4 independent experiments (separate platings) and statistical analysis was

performed by one-way repeated-measure ANOVA and the post hoc Tukey's test for multiple pairwise comparisons. For ELISA detection of the released BDNF, the values normalized to the basal value were averaged for 4 wells in one experiment. These values were then averaged for 4 independent experiments (separate platings) and statistical analysis was performed using one-way repeated-measure ANOVA and the post-hoc Tukey's test for multiple pairwise comparisons. Values of $p<0.05$ were considered significant.

Acknowledgments

This work was partly supported by a Grant-in-Aid for Young Scientists from the Ministry of Education, Science, Sports and Culture, Japan (KAKENHI 18700373), and a grant for Health Science Research Including Drug Innovation from the Japan Health Sciences Foundation awarded to K.S.; Health and Labour Science Research Grants for Research on Advanced Medical Technology from the Ministry of Health, Labour and Welfare, Japan, and a Grant-in-Aid for Scientific Research from the Ministry of Education, Science, Sports and Culture, Japan (KAKENHI 13672319), awarded to K.N.

Appendix A. Supplementary data

Supplementary data associated with this article can be found, in the online version, at doi:10.1016/j.brainres.2007.02.093.

REFERENCES

Acsady, L., Kamondi, A., Sik, A., Freund, T., Buzsaki, G., 1998. GABAergic cells are the major postsynaptic targets of mossy fibers in the rat hippocampus. J. Neurosci. 18, 3386–3403.

Aguado, F., Carmona, M.A., Pozas, E., Aguilo, A., Martinez-Guijarro, F.G., Alcantara, S., Borrell, V., Yuste, R., Ibanez, C.F., Soriano, E., 2003. BDNF regulates spontaneous correlated activity at early developmental stages by increasing synaptogenesis and expression of the K+/Cl– co-transporter KCC2. Development 130, 1267–1280.

Alsina, B., Vu, T., Cohen-Cory, S., 2001. Visualizing synapse formation in arborizing optic axons in vivo: dynamics and modulation by BDNF. Nat. Neurosci. 4, 1093–1101.

Balkowiec, A., Katz, D.M., 2002. Cellular mechanisms regulating activity-dependent release of native brain-derived neurotrophic factor from hippocampal neurons. J. Neurosci. 22, 10399–10407.

Beyer, C., Karolczak, M., 2000. Estrogenic stimulation of neurite growth in midbrain dopaminergic neurons depends on cAMP/protein kinase A signaling. J. Neurosci. Res. 59, 107–116.

Beyer, C., Ivanova, T., Karolczak, M., Kuppers, E., 2002. Cell type-specificity of nonclassical estrogen signaling in the developing midbrain. J. Steroid Biochem. Mol. Biol. 81, 319–325.

Beyer, C., Pawlak, J., Karolczak, M., 2003. Membrane receptors for oestrogen in the brain. J. Neurochem. 87, 545–550.

Bothwell, M., 1995. Functional interactions of neurotrophins and neurotrophins receptors. Annu. Rev. Neurosci. 18, 223–253.

Cambiasso, M.J., Carrer, H.F., 2001. Nongenomic mechanism mediates estradiol stimulation of axon growth in male rat hypothalamic neurons in vitro. J. Neurosci. Res. 66, 475–481.

Clarke, C.H., Norfleet, A.M., Clarke, M.S., Watson, C.S., 2000. Perimembrane localization of the estrogen receptor (protein in neuronal processes of cultured hippocampal neurons. Neuroendocrinology 71, 34–42.

Cochilla, A.J., Angleson, J.K., Betz, W.J., 1999. Monitoring secretory membrane with FM1-43 fluorescence. Ann. Rev. Neurosci. 22, 1–10.

Craven, S.D., Bredt, D.S., 1998. PDZ proteins organize synaptic signaling pathways. Cell 93, 495–509.

Danzer, S.C., McNamara, J.O., 2004. Localization of brain-derived neurotrophic factor to distinct terminals of mossy fiber axons implies regulation of both excitation and feedforward inhibition of CA3 pyramidal cells. J. Neurosci. 24, 11346–11355.

De Simoni, A., Griesinger, C.B., Edwards, F.A., 2003. Development of rat CA1 neurones in acute versus organotypic slices: role of experience in synaptic morphology and activity. J. Physiol. 550 (Pt. 1), 135–147.

Dieni, S., Rees, S., 2002. Distribution of brain-derived neurotrophic factor and TrkB receptor proteins in the fetal and postnatal hippocampus and cerebellum of the guinea pig. J. Comp. Neurol. 454, 229–240.

Duncia, J.V., Santella III, J.B., Higley, C.A., Pitts, W.J., Wityak, J., Frietze, W.E., Rankin, F.W., Sun, J.H., Earl, R.A., Tabaka, A.C., Teleha, C.A., Blom, K.F., Favata, M.F., Manos, E.J., Daulerio, A.J., Stradley, D.A., Horiuchi, K., Copeland, R.A., Scherle, P.A., Trzaskos, J.M., Magolda, R.L., Trainor, G.L., Wexler, R.R., Hobbs, F.W., Olson, R.E., 1998. MEK inhibitors: the chemistry and biological activity of U0126, its analogs, and cyclization products. Bioorg. Med. Chem. Lett. 8 (20), 2839–2844.

Garner, C.C., Nash, J., Huganir, R.L., 2000. PDZ domains in synapse assembly and signaling. Trends Cell Biol. 10, 274–280.

Gartner, A., Staiger, V., 2002. Neurotrophin secretion from hippocampal neurons evoked by long-term-potentiation-inducing electrical stimulation patterns. Proc. Natl. Acad. Sci. U. S. A. 99 (9), 6386–6391.

Germain, S.J., Campbell, P.S., Anderson, J.N., 1978. Role of the serum estrogen-binding protein in the control of tissue estradiol levels during postnatal development of the female rat. Endocrinology 103, 1401–1410.

Gould, E., Woolley, C.S., Frankfurt, M., McEwen, B.S., 1990. Gonadal steroids regulate dendritic spine density in hippocampal pyramidal cells in adulthood. J. Neurosci. 10, 1286–1291.

Hartmann, M., Heumann, R., Lessmann, V., 2001. Synaptic secretion of BDNF after high frequency stimulation of glutamatergic synapses. EMBO J. 20, 5887–5897.

Haubensak, W., Narz, F., Heumann, R., Lessmann, V., 1998. BDNF-GFP containing secretory granules are localized in the vicinity of synaptic junctions of cultured cortical neurons. J. Cell Sci. 111, 1483–1493.

Hojo, Y., Hattori, T., Enami, T.A., Hurukawa, A., Suzuki, K., Ishii, H.T., Mukai, H., Morrison, J.H., Janssen, W.G., Kominami, S., Harada, N., Kimoto, T., Kawato, S., 2004. Adult male rat hippocampus synthesizes estradiol from pregnenolone by cytochromes P45017α and P450 aromatase localized in neurons. Proc. Natl. Acad. Sci. U. S. A. 101, 865–870.

Ikegaya, Y., Nishiyama, N., Matsuki, N., 2000. L-type Ca^{2+} channel blocker inhibits mossy fiber sprouting and cognitive deficits following pilocarpine seizures in immature mice. Neuroscience 98, 647–659.

Ivanova, T., Kuppers, E., Engele, J., Beyer, C., 2001. Estrogen stimulates brain-derived neurotrophic factor expression in embryonic mouse midbrain neurons through a membrane-mediated and calcium-dependent mechanism. J. Neurosci. Res. 66, 221–230.

Jontes, J.D., Smith, S.J., 2000. Filopodia, spines, and the generation of synaptic diversity. Neuron 27, 11–14.

Kase, H., Iwahashi, K., Nakanishi, S., Matsuda, Y., Yamada, K., Takahashi, M., Murakata, C., Sato, A., Kaneko, M., 1987. K-252 compounds, novel and potent inhibitors of protein kinase C

and cyclic nucleotide-dependent protein kinases. Biochem. Biophys. Res. Commun. 142, 436–440.
Kay, A.R., Alfonso, A., Alford, S., Cline, H.T., Holgado, A.M., Sakmann, B., Snitsarev, V.A., Stricker, T.P., Takahashi, M., Wu, L.G., 1999. Imaging synaptic activity in intact brain and slices with FM1-43 in *C. elegans*, lamprey, and rat. Neuron 24, 809–817.
Kelly, M.J., Levin, E.R., 2001. Rapid actions of plasma membrane estrogen receptors. Trends Endocrinol. Metab. 12, 152–156.
Koyama, R., Yamada, M.K., Fujisawa, S., Katoh-Semba, R., Matsuki, N., Ikegaya, Y., 2004. Brain-derived neurotrophic factor induces hyperexcitable reentrant circuits in the dentate gyrus. J. Neurosci. 24, 7215–7224.
Kramar, E.A., Lin, B., Lin, C.Y., Arai, A.C., Gall, C.M., Lynch, G., 2004. A novel mechanism for the facilitation of theta-induced long-term potentiation by brain-derived neurotrophic factor. J. Neurosci. 24 (22), 5151–5161.
Kretz, O., Fester, L., Wehrenberg, U., Zhou, L., Brauckmann, S., Zhao, S., Prange-Kiel, J., Naumann, T., Jarry, H., Frotscher, M., Rune, G.M., 2004. Hippocampal synapses depend on hippocampal estrogen synthesis. J. Neurosci. 24, 5913–5921.
Kuiper, G.G., Carlsson, B., Grandien, K., Enmark, E., Haggblad, J., Nilsson, S., Gustafsson, J.A., 1997. Comparison of the ligand binding specificity and transcript tissue distribution of estrogen receptors alpha and beta. Endocrinology 138, 863–870.
Lawrence, J.J., McBain, C.J., 2003. Interneuron diversity series: containing the detonation-feedforward inhibition in the CA3 hippocampus. Trends Neurosci. 26, 631–640.
Lessmann, V., Gottmann, K., Malcangio, M., 2003. Neurotrophin secretion: current facts and future prospects. Prog. Neurobiol. 69, 341–374.
Matsunaga, W., Shirokawa, T., Isobe, S., 2004. BDNF is necessary for maintenance of noradrenergic innervations in the aged rat brain. Neurobiol. Aging 25, 341–348.
McAllister, A.K., Katz, L.C., Lo, D.C., 1999. Neurotrophins and synaptic plasticity. Annu. Rev. Neurosci. 22, 295–318.
McEwen, B., Akama, K., Alves, S., Brake, W.G., Bulloch, K., Lee, S., Li, C., Yuen, G., Milner, T.A., 2001. Tracking the estrogen receptor in neuron: implication for estrogen-induced synapse formation. Proc. Natl. Acad. Sci. U. S. A. 98, 7093–7100.
Mizuhashi, S., Nishiyama, N., Matsuki, N., Ikegaya, Y., 2001. Cyclic nucleotide-mediated regulation of hippocampal mossy fiber development: a target-specific guidance. J. Neurosci. 15 21 (16), 6181–6194.
Murphy, D.D., Cole, N.B., Greenberger, V., Segal, M., 1998a. Estradiol increases dendritic spine density by reducing GABA neurotransmission in hippocampal neurons. J. Neurosci. 18 (7), 2550–2559.
Murphy, D.D., Cole, N.B., Segal, M., 1998b. Brain-derived neurotrophic factor mediates estradiol-induced dendritic spine formation in hippocampal neurons. Proc. Natl. Acad. Sci. U. S. A. 95 (19), 11412–11417.
Nakagami, Y., Saito, H., Matsuki, N., 1997. The regional vulnerability to blockade of action potentials in organotypic hippocampal culture. Brain Res. Dev. Brain Res. 103 (1), 99–102.
Okabe, S., Miwa, A., Okado, H., 2001. Spine formation and correlated assembly of presynaptic and postsynaptic molecules. J. Neurosci. 21, 6105–6114.
Patterson, S.L., Pittenger, C., Morozov, A., Martin, K.C., Scanlin, H., Drake, C., Kandel, E.R., 2001. Some forms of cAMP-mediated long-lasting potentiation are associated with release of BDNF and nuclear translocation of phospho-MAP kinase. Neuron 32, 123–140.
Pozzo-Miller, L.D., Inoue, T., Murphy, D.D., 1999. Estradiol increases spine density and NMDA-dependent Ca^{2+} transients in spines of CA1 pyramidal neurons from hippocampal slices. J. Neurophysiol. 81, 1404–1411.
Qin, L., Marrs, G.S., Mckim, R., Dailey, M.E., 2001. Hippocampal mossy fibers induce assembly and clustering of PSD95-containing postsynaptic densities independent of glutamate receptor activation. J. Comp. Neurol. 440, 284–298.
Rasika, S., Alvarez-Buylla, A., Nottebohm, F., 1999. BDNF mediates the effects of testosterone on the survival of new neurons in an adult brain. Neuron 22, 53–62.
Razandi, M., Pedram, A., Merchenthaler, I., Greene, G.L., Levin, E.R., 2004. Plasma membrane estrogen receptors exist and functions as dimmers. Mol. Endocrinol. 18, 2854–2865.
Rothermel, J.D., Parker Botelho, L.H., 1988. A mechanistic and kinetic analysis of the interactions of the diastereoisomers of adenosine 3′,5′-(cyclic)phosphorothioate with purified cyclic AMP-dependent protein kinase. Biochem. J. 251, 757A–762A.
Sato, K., Matsuki, N., Ohno, Y., Nakazawa, K., 2002. Effects of 17β-estradiol and xenoestrogens on the neuronal survival in an organotypic hippocampal culture. Neuroendocrinology 76, 223–234.
Scharfman, H.E., MacLusky, N.J., 2005. Similarities between actions of estrogen and BDNF in the hippocampus: coincidence or clue? Trends Neurosci. 28 (2), 79–85.
Scharfman, H.E., Mercurio, T.C., Goodman, J.H., Wilson, M.A., MacLusky, N.J., 2003. Hippocampal excitability increases during the estrous cycle in the rat: a potential role for brain-derived neurotrophic factor. J. Neurosci. 23, 11641–11652.
Segal, M., Murphy, D., 2001. Estradiol induces formation of dendritic spines in hippocampal neurons: functional correlates. Horm. Behav. 40 (2), 156–159.
Segars, J.H., Driggers, P.H., 2002. Estrogen action and cytoplasmic signaling cascades. Part I: membrane-associated signaling complexes. Trends Endocrinol. Metab. 13, 349–354.
Seil, F.J., Drake-Baumann, R., 2000. TrkB receptor ligands promote activity-dependent inhibitory synaptogenesis. J. Neurosci. 20, 5367–5373.
Sohrabji, F., Miranda, R.C., Toran-Allerand, C.D., 1995. Identification of a putative estrogen response element in the gene encoding brain-derived neurotrophic factor. Proc. Natl. Acad. Sci. U. S. A. 92, 11110–11114.
Squinto, S.P., Stitt, T.N., Aldrich, T.H., Davis, S., Bianco, S.M., Radziejewski, C., Glass, D.J., Masiakowski, P., Furth, M.E., Valenzuela, D.M., Distefano, P.S., Yancopolous, G.D., 1991. trkB encodes a functional receptor for brain-derived neurotrophic factor and neurotrophin-3 but not nerve growth factor. Cell 65, 885–893.
Tait, R.J., Skanchy, D.J., Thompson, D.P., Chetwyn, N.C., Dunshee, D.A., Rajewski, R.A., Stella, V.J., Stobaugh, J.F., 1992. Characterization of sulfoalkyl ether derivatives of beta-cyclodextrin by capillary electrophoresis with indirect UV detection. J. Pharm. Biomed. Anal. 10, 615–622.
Takahashi, H., Sekino, Y., Tanaka, S., Mizui, T., Kishi, S., Shirao, T., 2003. Drebrin-dependent actin clustering in dendritic filopodia governs synaptic targeting of postsynaptic density-95 and dendritic spine morphogenesis. J. Neurosci. 23, 6586–6595.
Tanapat, P., Hastings, N.B., Reeves, A.J., Gould, E., 1999. Estrogen stimulates a transient increase in the number of new neurons in the dentate gyrus of the adult female rat. J. Neurosci. 19 (14), 5792–5801.
Thomas, P., Pang, Y., Filardo, E.J., Dong, J., 2004. Identity of an estrogen membrane receptor coupled to a G-protein in human breast cancer cells. Endocrinology 146, 624–632.
Toran-Allerand, C.D., Guan, X., MacLusky, N.J., Horvath, T.L., Diano, S., Singh, M., Connolly Jr., E.S., Nethrapalli, I.S., Tinnikov, A.A., 2002. ER-X: a novel, plasma membrane-associated, putative estrogen receptor that is regulated during development and after ischemic brain injury. J. Neurosci. 22, 8391–8401.
Tyler, W.J., Alonso, M., Bramham, C.R., Pozzo-Miller, L.D., 2002. From acquisition to consolidation: on the role of brain-derived neurotrophic factor signaling in hippocampal-dependent learning. Learn. Mem. 9 (5), 224–237.
Woolley, C.S., 1998. Estrogen-mediated structural and functional

synaptic plasticity in the female rat hippocampus. Horm. Behav. 34 (2), 140–148.
Woolley, C.S., Schwartzkroin, P.A., 1998. Hormonal effects on the brain. Epilepsia 39 (Suppl. 8), S2–S8.
Wu, Y.J., Kruttgen, A., Moller, J.C., Shine, D., Chan, J.R., Shooter, E.M., Cosgaya, J.M., 2004. Nerve growth factor, brain-derived neurotrophic factor, and neurotrophin-3 are sorted to dense-core vesicles and released via the regulated pathway in primary rat cortical neurons. J. Neurosci. Res. 75, 825–834.
Znamensky, V., Akama, K.T., McEwen, B., Milner, T., 2003. Estrogen levels regulate the subcellular distribution of phosphorylated Akt in hippocampal CA1 dendrites. J. Neurosci. 23, 2340–2347.

Neuroscience 147 (2007) 153–163

RETINOIC ACIDS ACTING THROUGH RETINOID RECEPTORS PROTECT HIPPOCAMPAL NEURONS FROM OXYGEN-GLUCOSE DEPRIVATION-MEDIATED CELL DEATH BY INHIBITION OF C-JUN-N-TERMINAL KINASE AND p38 MITOGEN-ACTIVATED PROTEIN KINASE

Y. SHINOZAKI,[a] Y. SATO,[b]* S. KOIZUMI,[a] Y. OHNO,[c] T. NAGAO[c] AND K. INOUE[d]

[a]*Division of Pharmacology, National Institute of Health Sciences, 1-18-1 Kamiyoga, Setagaya, Tokyo 158-8501, Japan*

[b]*Division of Cellular and Gene Therapy Products, National Institute of Health Sciences, 1-18-1 Kamiyoga, Setagaya, Tokyo 158-8501, Japan*

[c]*National Institute of Health Sciences, 1-18-1 Kamiyoga, Setagaya, Tokyo 158-8501, Japan*

[d]*Department of Molecular and System Pharmacology, Graduate School of Pharmaceutical Sciences, Kyushu University, Maidashi3-1-1, Higashi-ku, Fukuoka 812-8582, Japan*

Abstract—Retinoic acids (RAs), including all-*trans* retinoic acid (ATRA) and 9-*cis* retinoic acid (9-*cis* RA), play fundamental roles in a variety of physiological events in vertebrates, through their specific nuclear receptors: retinoic acid receptor (RAR) and retinoid X receptor (RXR). Despite the physiological importance of RA, their functional significance under pathological conditions is not well understood. We examined the effect of ATRA on oxygen/glucose-deprivation/reperfusion (OGD/Rep)-induced neuronal damage in cultured rat hippocampal slices, and found that ATRA significantly reduced neuronal death. The cytoprotective effect of ATRA was observed not only in cornu ammonis (CA) 1 but also in CA2 and dentate gyrus (DG), and was attenuated by selective antagonists for RAR or RXR. By contrast, in the CA3 region, no protective effects of ATRA were observed. The OGD/Rep also increased phosphorylated forms of c-jun-N-terminal kinase (P-JNK) and p38 (P-p38) in hippocampus, and specific inhibitors for these kinases protected neurons. ATRA prevented the increases in P-JNK and P-p38 after OGD/Rep, as well as the decrease in NeuN and its shrinkage, all of which were inhibited by antagonists for RAR or RXR. These findings suggest that the ATRA signaling via retinoid receptors results in the inhibition of JNK and p38 activation, leading to the protection of neurons against OGD/Rep-induced damage in the rat hippocampus.

*Corresponding author. Tel: +81-3-3700-1141x275; fax: +81-3-3707-6950.
E-mail address: yoji@nihs.go.jp (Y. Sato).

Abbreviations: ATRA, all-*trans* retinoic acid; CA, cornu ammonis; DG, dentate gyrus; ERK, extracellular signal-regulated kinase; Hanks' BSS, Hanks' balanced salt solution; JNK, c-jun-N-terminal kinase; MAPK, mitogen-activated protein kinase; MKP-1, mitogen-activated protein kinase phosphatase-1; OGD, oxygen and glucose deprivation; PBS-T, phosphate-buffered saline with 0.3% Triton X-100, pH 7.6; P-ERK, phosphorylated extracellular signal-regulated kinase; PI, propidium iodide; P-JNK, phosphorylated c-jun-N-terminal kinase; P-p38, phosphorylated p38; RA, retinoic acid; RAR, retinoic acid receptor; Rep, reperfusion; RXR, retinoid X receptor; ssDNA, single-stranded DNA; TBS/T, Tris-buffered saline containing 0.1% Tween-20; 9-*cis* RA, 9-*cis* retinoic acid.

Key words: retinoic acid, RAR, RXR, MAPK, ischemia.

Retinoids, including vitamin A (retinol) and its derivatives, regulate a wide range of biological processes, such as cell growth and differentiation, development, and carcinogenesis (Chambon, 1996; Maden, 2001). Retinoic acids (RAs) regulate the expression of a large number of genes upon binding and activation of the nuclear retinoid receptors, retinoic acid receptors (RARα, RARβ, and RARγ) and retinoid X receptors (RXRα, RXRβ, and RXRγ) (Chambon, 1996; Maden, 2001). RARs are activated by all-*trans* retinoic acid (ATRA) and 9-*cis* retinoic acid (9-*cis* RA), whereas RXRs are activated by 9-*cis* RA (Chambon, 1996) and other non-retinoid lipid ligands such as docosahexaenoic acid (de Urquiza et al., 2000). In the presence of RA, these receptors act as transcription factors in forms of RAR/RXR heterodimers or RXR homodimers, which bind to retinoic acid response elements (RARE) in the promoter of target genes (Chambon, 1994; Kastner et al., 1997). RA has multiple effects on physiological functions in the adult brain, such as long-term potentiation and long-term depression (Chiang et al., 1998; Misner et al., 2001) and neurogenesis (Haskell and LaMantia, 2005; Jacobs et al., 2006). RA also plays significant roles under pathological conditions. For example, in mesangial cells and fibroblast, ATRA has a protective effect against H_2O_2 via receptor-mediated mechanisms (Konta et al., 2001; Xu et al., 2002). Although several lines of evidence link RA to some psychiatric pathogenesis (Strahan and Raimer, 2006), defects in retinoid signaling have been associated with neurodegenerative disorders such as Alzheimer's disease and amyotrophic lateral sclerosis (Corcoran et al., 2002; Goodman and Pardee, 2003). However, the role of RA signaling in other pathological conditions such as ischemia in the brain remains unclear.

The mitogen-activated protein kinase (MAPK) family, which plays an essential role in the transduction of environmental stimuli to the nucleus, consists of three commonly recognized subgroups: extracellular signal-regulated kinase (ERK), c-jun-N-terminal kinase (JNK), also known as the stress activated protein kinase (SAPK) and p38 kinase. JNK and p38 kinase are activated in response to cellular stresses like ischemia in the heart, kidney and brain (Hu and Wieloch, 1994; Mizukami et al., 1997; Yin et al., 1997; Herdegen et al., 1998; Walton et al., 1998) and have been associated with neuronal cell death (Xia et al., 1995; Watson et al., 1998; Namgung and Xia, 2000). JNK

0306-4522/07$30.00+0.00
doi:10.1016/j.neuroscience.2007.04.032

and p38 kinase activate downstream molecules such as caspase-3 (Kuan et al., 2003; Lee and Lo, 2003), Bax (Okuno et al., 2004), MAPK-activated protein kinase 2 (MAPKAP2) (Wang et al., 2002) and activator protein-1 (AP-1) (Ishikawa et al., 1997; Yokoo and Kitamura, 1997; Behrens et al., 1999) thereby leading of neuronal cell death. In contrast, ERK1/2 is mainly activated by various neurotransmitters, hormones and growth factors, controlling transcription factor activity to induce various physiological responses, such as cell proliferation or differentiation (Boulton et al., 1991; Marshall, 1995; Segal and Greenberg, 1996). However, ERK1/2 is also activated by various types of stress such as oxidative or shear stress, controlling the survival of cells (Xia et al., 1995; Guyton et al., 1996; Wang et al., 1998). Recent studies have shown that ATRA protects neurons from amyloidβ (Sahin et al., 2005) and staurosporine (Ahlemeyer and Krieglstein, 1998). Based on the findings above, we hypothesized that RA signaling would be inversely associated with neuronal cell death under pathological conditions. To test our hypothesis, we examined the effect of ATRA on hippocampal neurons against oxygen and glucose deprivation/reperfusion (OGD/Rep)-induced neuronal damage, and found that ATRA protected hippocampal neurons against cell death. We also found that the neuroprotective effect of ATRA was mediated by inhibition of OGD/Rep-induced activation of JNK and p38 kinase.

EXPERIMENTAL PROCEDURES

Materials

Propidium iodide (PI) and anti-β-actin antibody were purchased from Sigma Chemical Co. (St. Louis, MO, USA). The sources of the following chemicals are shown in parentheses: ATRA and 9-*cis* RA (Wako Pure Chemicals, Osaka, Japan), U0126, SB203580, SP600125 and anti-NeuN antibody (Calbiochem Biosciences, Inc., San Diego, CA, USA). LE135 (Li et al., 1999) and HX531 (Ebisawa et al., 1999) were synthesized and graciously provided by Dr. Koichi Shudo (Research Foundation Itsuu Laboratory, Tokyo, Japan). Antibodies against phosphorylated extracellular signal-regulated kinase 1/2 (P-ERK1/2), phosphorylated p38 (P-p38), phosphorylated c-jun-N-terminal kinase (P-JNK), and active caspase-3 were purchased from Cell Signaling Technology (Beverly, MA, USA). The sources of the following antibodies are shown in parentheses: single-stranded DNA (ssDNA) antibody (DAKO Cytomation, Glostrup, Denmark), RAR and RXR antibodies (Santa Cruz Biotechnology, Inc., Santa Cruz, CA, USA).

Organotypic hippocampal slice culture

Organotypic slice cultures of the hippocampus were prepared using the culture method described by Skrede and Westgaard (1971) All animals were treated in accordance with the laboratory animal care guidance of the National Institute of Health Sciences at Tokyo and the guidelines of the International Council for Laboratory Animal Science (ICLAS; http://www.iclas.org/). Every effort was made to minimize the number of experimental animals used and their suffering. Eleven-day-old Wistar rats were decapitated, and the brains were rapidly dissected and placed in a Petri dish containing ice-cold 1× Hanks' balanced salt solution (Hanks' BSS, from Gibco, Rockville, MD, USA). Both right and left hippocampi were isolated and sectioned into 300 μm transverse slices with a McIlwain tissue chopper (Mickle Laboratory Engineering Co. Ltd., Goose Green, UK). The slices were then carefully separated and transferred onto porous membrane inserts of six-well culture plates (two or three slices per insert) (Millicell-CM, Millipore, Billerica, MA, USA). To reach the level of insert membrane, 800 μL culture medium was added to the lower compartment of each well, and the culture plates were then placed in a 37 °C humidified incubator enriched with 5% CO_2. The cell culture medium consisted of 50% Minimum Essential Medium with 25 mM Hepes, 25% Hanks' BSS and 25% heat-inactivated horse serum, which were supplemented with 2 mM L-glutamine, 100 U/mL penicillin and 100 μg/mL streptomycin. On the next day, the culture medium was replaced with fresh medium and from then on changed once every 2 days. Hippocampal slices were used for each experiment after incubation for 12 days.

OGD

Hippocampal slices were exposed to OGD using an anaerobic chamber. The slices were transferred in dishes with 800 μl glucose-free DMEM containing (mg/L): 200 $CaCl_2$, 400 KCl, 97.67 $MgSO_4$, 6400 NaCl, 3700 $NaHCO_3$, 125 NaH_2PO_4 and then placed into an airtight chamber containing 95% N_2, 5% CO_2 (37 °C) for 40 min. After OGD, the slices were placed back in the incubator in normal culture medium and incubated for 24 h. RAs were added to the culture medium 24 h before OGD and during Rep. Antagonists for RAR and RXR were added to the medium 30 min before and during the RA treatment. Inhibitors of MAPKs were added to the slices simultaneously at Rep.

Immunohistochemistry

The hippocampal slices were fixed with 4% paraformaldehyde for 1–2 h and rinsed two times (each 10 min at room temperature) with PBS-T (phosphate-buffered saline with 0.3% Triton X-100, pH 7.6). After blocking with 3% normal goat serum in PBS-T for 2 h at room temperature, the slices were incubated with the primary antibody (1/1000-fold dilution in PBS-T with 3% goat serum) for 48 h at 4 °C, followed by incubation with the Alexa Fluor-conjugated secondary antibody (1/1000-fold dilution, Molecular Probes, Eugene, OR, USA) for 3 h at room temperature. Images were collected with a MRC-1024 laser-scanning microscope (Bio-Rad, Richmond, CA, USA) using ×4 or ×20 objective lenses. For comparisons of double-stained patterns, images were processed using Photoshop CS (Adobe Systems, Mountain View, CA, USA). High magnification images of the NeuN/active caspase-3/ssDNA/P-p38/P-JNK staining are shown for the cornu ammonis 1 (CA1) region, unless otherwise indicated.

Western blotting analysis of slices

Slices were homogenized in 100 μl lysis buffer (10 mM Tris, pH 7.5, 150 mM NaCl, 1 mM EDTA, 1 mM EGTA, 1% Triton X-100, 0.1% SDS, 1 mM sodium orthovanadate, 1% deoxycholate, and 10 μg/mL each aprotinin, bestatin, pepstatin A, leupeptin), using Tissue Lyser (Qiagen, Hilden, Germany). The proteins were separated in 10% SDS-PAGE gels and transferred to PVDF membranes. The membranes were blocked for 1 h in Tris-buffered saline containing 0.1% Tween-20 (TBS/T) and 5% non-fat dry milk at room temperature. Then the membranes were incubated with the primary antibody (1/1000-fold dilution in TBS/T containing 5% BSA) overnight at 4 °C. After three washes with TBS/T, the membranes were incubated with a horseradish peroxidase–conjugated anti-rabbit antibody (1/2000 dilution in TBS/T containing 5% non-fat dry milk) for 1 h at room temperature. The membranes were washed with TBS/T three times, and the proteins were visualized by chemiluminescence.

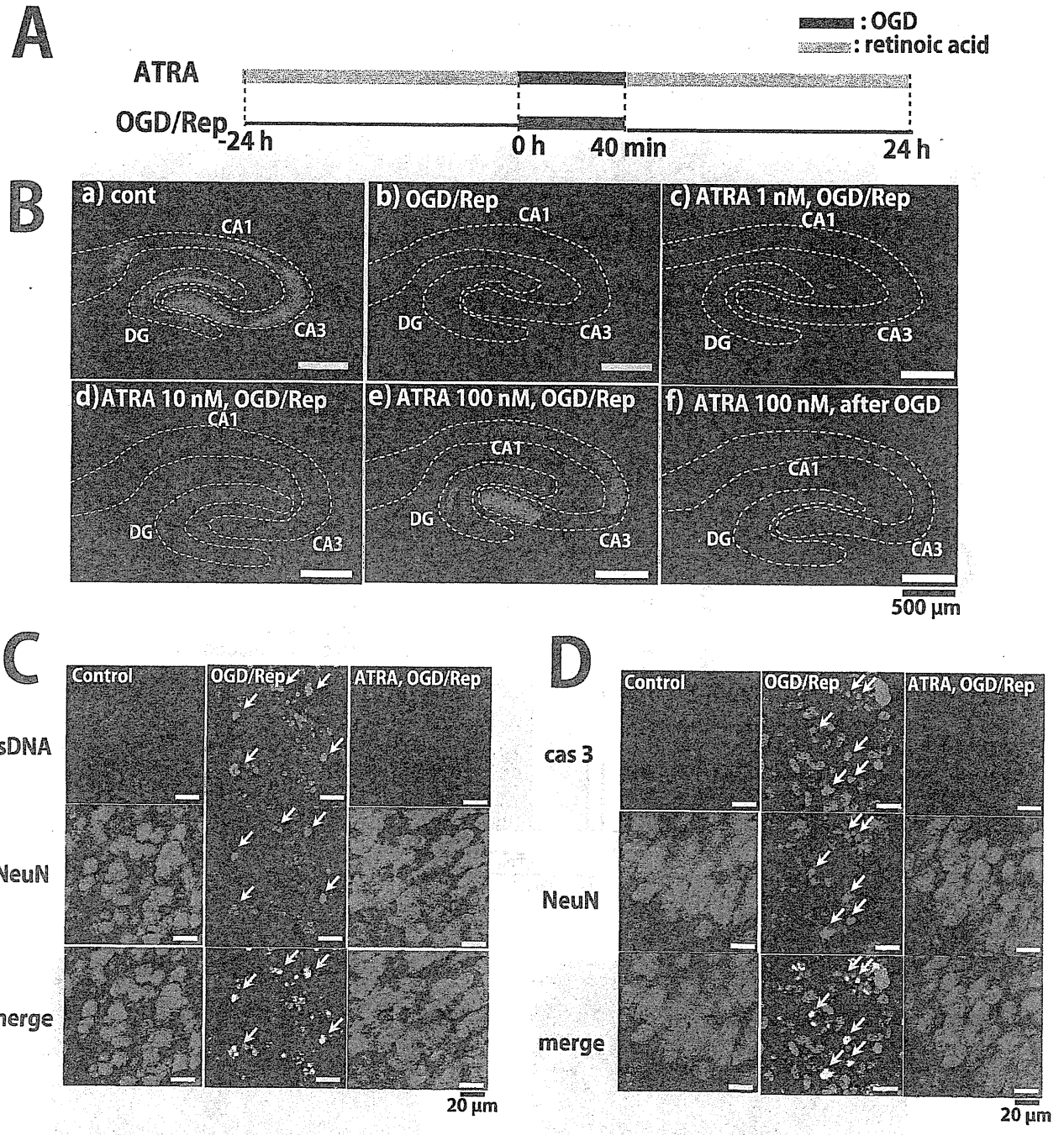

Fig. 1. The protective effect of ATRA on OGD/Rep-induced damage of neurons in the organotypic hippocampal slice culture. (A) A schematic diagram of the experimental protocol. Hippocampal slices were treated with ATRA 24 h before OGD and during Rep. The slices were subjected to OGD for 40 min followed by 24 h Rep. (B) The protective effect of ATRA on neurons in hippocampal slices. (a) NeuN staining of control slices. Incubation period for 12 days did not affect the NeuN staining of hippocampal slices. (b) OGD/Rep-induced neuronal loss. OGD/Rep dramatically decreased NeuN staining in hippocampal slices. (c–e) Effect of ATRA on the OGD/Rep-induced decrease of NeuN staining in hippocampal slices. At 1 nM, ATRA did not have a significant effect on NeuN staining decreased by OGD/Rep (c). At ≥10 nM ATRA prevented the decrease in NeuN by OGD/Rep (d, 10 nM; e, 100 nM). (f) The protective effect of ATRA after OGD. ATRA (100 nM) after OGD also had protective effects. Scale bar=500 μm. (C) DNA damage associated with the OGD/Rep-induced decrease in NeuN. In control, ssDNA signals were hardly detected (left, upper panel). OGD/Rep increased ssDNA signals (center, upper panel), which were shrunken and merged with NeuN signals (center, lower panel, arrows). ATRA prevented the changes in NeuN signals (right, middle panel) and reversed the increased ssDNA signals (right, upper panel). (D) OGD/Rep activates caspase-3 in neuronal cells. In control, the signals for active caspase-3 were barely detected (left, upper panel). OGD/Rep induced an increase in active caspase-3 (center, upper panel), which was colocalized with NeuN signals (center, arrows). ATRA prevented the OGD/Rep-induced changes in NeuN and active caspase-3 (right, middle and upper panels). Scale bar=20 μm.

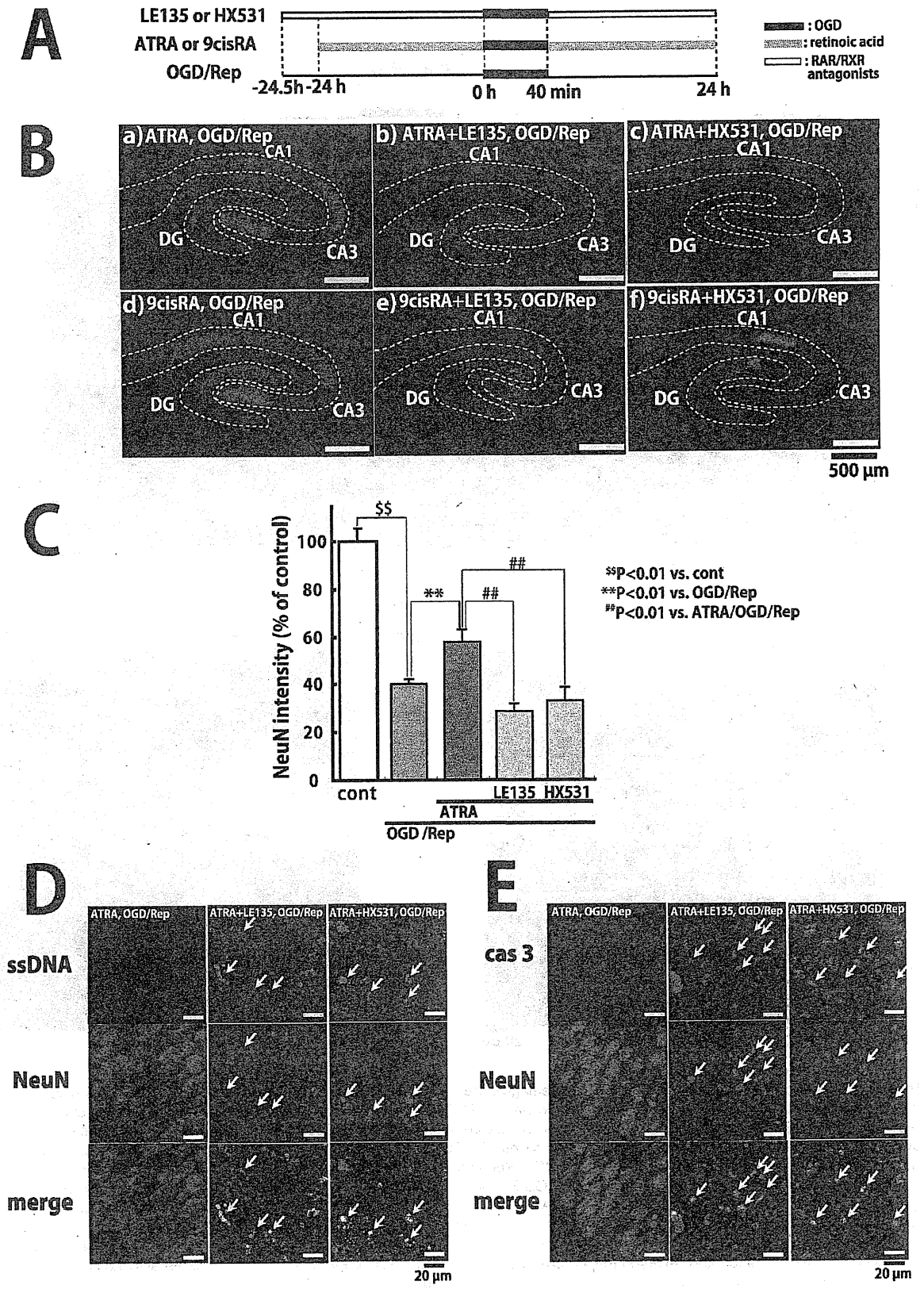

Fig. 2. The inhibitory effect of RAR/RXR antagonists on the RA-induced protective effect. (A) A schematic diagram of the experimental protocol. Hippocampal slices were treated with RAs (ATRA or 9-*cis* RA) 24 h before OGD and during Rep. Antagonists for RAR and RXR were added to the culture medium 30 min before and during RA treatment. The slices were subjected to OGD for 40 min and Rep for 24 h. (B) RAR/RXR antagonists inhibit the neuroprotective effect of RA. The effect of ATRA (a) was inhibited by both RAR antagonist LE135 (1 μM) (b) and RXR antagonist HX531

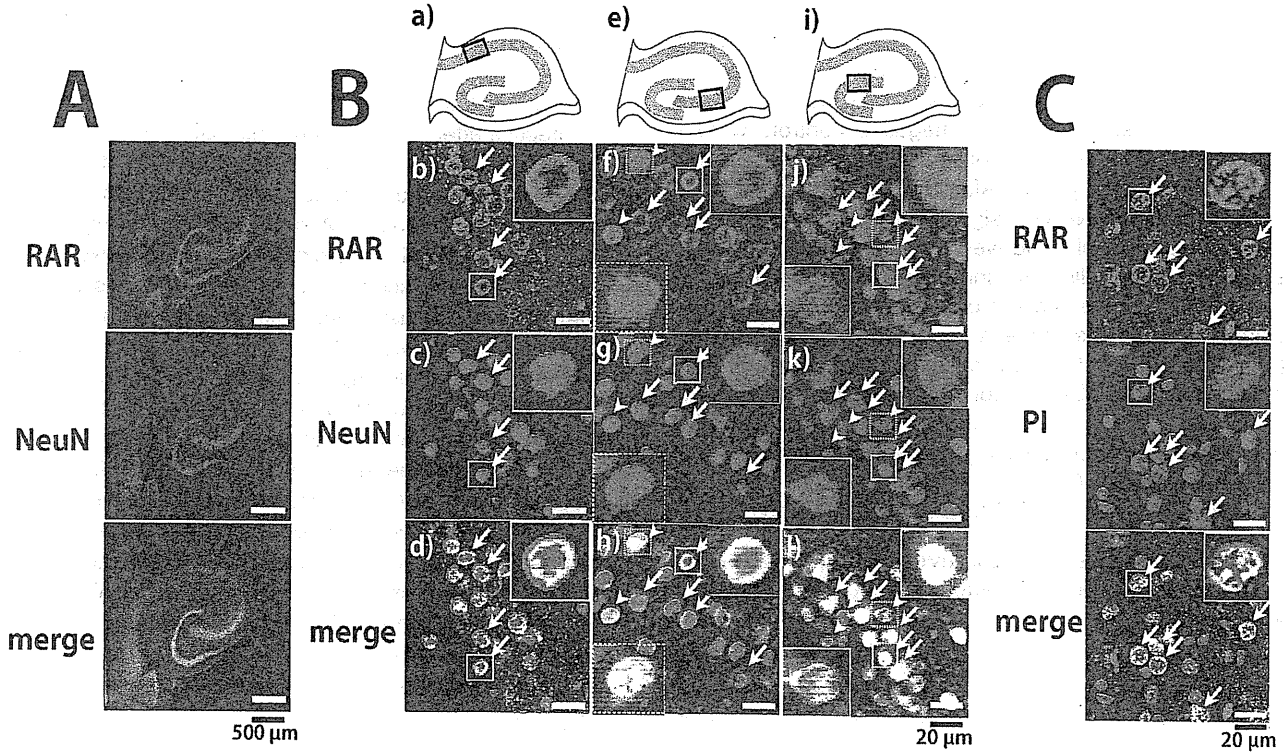

Fig. 3. Subregional expression pattern of RAR in the hippocampus. (A) Immunostaining for RAR showed a neuronal cell layer-like pattern in CA1 to CA3 and in DG (upper panel). The RAR signals were clearly colocalized with those for NeuN (lower panel). Scale bar=500 μm. (B) Differences in the expression pattern of RAR between subregions of the hippocampus. Images in b–d were obtained from the CA1 region indicated by the square in a. The signals for RAR appeared in ring-forms in CA1 (b; arrows). The signals for NeuN (c) were colocalized with those for RAR (d). Images in f–h were obtained from the CA3 region indicated by the square in e. In the CA3 region, RAR signals were mainly in ring-forms (f; arrows) but a few were in diffusion-forms (f; arrowheads), which were colocalized with those for NeuN (g, h). Images in j–l were obtained from the DG region indicated by the square in i. The RAR signals in DG were observed mainly in diffusion-forms (j; arrows) with a few RARs in ring-forms (j; arrowheads), which were colocalized with the NeuN signals (k, l). (C) RARs exist in the nucleus. RARs in CA1 were colocalized with PI signals (arrows). The insets show high-magnified images of square-selected region. Scale bar=20 μm.

Quantification of the immunostaining

The intensity of NeuN, which is not only a marker for neuronal nuclei but also for neuronal viability in hippocampus (Nakatomi et al., 2002; Liu et al., 2004; Gao et al., 2005), was quantified using Image J software (http://rsb.info.nih.gov/ij/) (Lyuksyutova, 2003; MacDonald, 2006). The center parts of the neuronal cell layers from CA1 to CA3 or dentate gyrus (DG) were traced and analyzed (analysis-measure) by "line selection from tool bar" and the NeuN intensity was measured by "Analysis-measure" from the menu bar. The mean value was employed as the intensity of the signal.

Statistics

Data were expressed mean±S.E.M. unless otherwise indicated. Data were analyzed for statistical significance by ANOVA followed by Student-Neuman-Keuls post hoc test. Significance was imparted at the $P<0.05$ level.

RESULTS

The protective effect of RA on OGD/Rep-induced neuronal loss of hippocampal slice

Fig. 1A shows the experimental procedure in the present study. The neuronal cell layer of hippocampal slice cultures 12 days after dissection from 11-day-old rats is shown in Fig. 1B(a). The neuronal cell layer was confirmed by immunohistochemistry using an antibody against NeuN. OGD for 40 min and Rep for 24 h shrank the NeuN signal, which also decreased its intensity significantly (Fig. 1B(b)). Hippocampal slices were treated with ATRA 24 h before OGD/Rep. The decrease in the NeuN signal intensity by OGD/Rep was prevented by ATRA at ≥10 nM (Fig. 1B(c–e)). In addition to the pre-treatment, post-treatment with ATRA

(1 μM) (c). 9-*cis* RA also showed the protective effect on neuronal cells against OGD/Rep-induced damage (d). The protective effect of 9-*cis* RA was inhibited by LE135 (1 μM) (e) and HX531 (1 μM) (f). Scale bar=500 μm. (C) Quantification of the signals for NeuN. OGD/Rep decreased the NeuN intensity to 40% of the controls, which was restored to 60% by ATRA (100 nM, 24 h). The effect of ATRA was offset by LE135 (1 μM) or HX531 (1 μM). Values were expressed as mean±S.E.M. (n=6~8). $^{\$\$}$ $P<0.01$ vs. control. ** $P<0.01$ vs. OGD/Rep. $^{\#\#}$ $P<0.01$ vs. ATRA/OGD/Rep. (D) RAR/RXR antagonists aggravate DNA damage of neurons. The ATRA-mediated inhibition of the OGD/Rep-increased ssDNA signals (left, upper panel) as well as on the shrinkage of NeuN (left, middle panel), was diminished in the presence of LE135 (1 μM; center) or HX531 (1 μM; right). Signals for NeuN were colocalized with ssDNA signals (lower panels, arrows). (E) RAR/RXR antagonists aggravate caspase-3 activation by OGD/Rep. The inhibitory effect of ATRA on the OGD/Rep-induced increase in active caspase-3 (left, upper panel) was diminished in the presence of LE135 (1 μM; center) or HX531 (1 μM; right). NeuN (middle panels) was colocalized with active caspase-3 (lower panels). Scale bar=20 μm.

after OGD was also cytoprotective (Fig. 1B(f)). As DNA damage is a marker of ischemia-induced neuronal cell death (Kawase et al., 1999) and caspase-3 activation (Chen et al., 1998), we employed antibodies for ssDNA and active caspase-3. In the negative controls without OGD/Rep, immunostaining for ssDNA was hardly detected (Fig. 1C left, upper panel). After the OGD/Rep, the immunostaining for ssDNA was significantly enhanced (Fig. 1C center, upper panel). The NeuN signals were detected in ssDNA-positive cells and shrunken (Fig. 1C center, arrows). ATRA prevented not only the increases in ssDNA signals but also the decrease in NeuN and its shrinkage (Fig. 1C right). Cells positive for active caspase-3 were detected after OGD/Rep but not in the controls without OGD/Rep (Fig. 1D, upper panels). The signals for active caspase-3 in the OGD/Rep group were colocalized with the NeuN signals. ATRA prevented caspase-3 activation, as well as the shrinkage of NeuN signals (Fig. 1D, right).

The inhibitory effect of selective RAR and RXR antagonists on the ATRA-induced neuroprotection against OGD/Rep

We next examined whether the protective effect of ATRA was mediated by RAR and/or RXR. Hippocampal slices were treated with ATRA 24 h before OGD and during Rep (Fig. 2A). Antagonists for RAR and RXR were added to the culture medium 30 min before ATRA treatment. As shown in Fig. 2B, both a specific RAR antagonist LE135 (1 μM) and a specific RXR antagonist HX531 (1 μM) inhibited the protective effect of ATRA (100 nM, 24 h) (Fig. 2B(b, c)). In addition, 9-*cis* RA (100 nM) had a protective effect against OGD/Rep-induced neuronal death (Fig. 2B(d)), which was reversed by LE135 (1 μM) or HX531 (1 μM) (Fig. 2B(e, f)). LE135 and HX531 alone did not attenuate the NeuN signal in hippocampal slices (data not shown). Based on quantitative analyses using the Image J program, OGD/Rep appeared to decrease the intensity of the NeuN signal to 40% of the controls (Fig. 2C). ATRA (100 nM) significantly inhibited the effect of OGD/Rep on the NeuN intensity, which was reversed by LE135 (1 μM) and HX531 (1 μM). To confirm that the effect on NeuN reflected the cytoprotective activity of ATRA, hippocampal slices were simultaneously stained with specific antibodies for NeuN, ssDNA and active caspase-3. As shown in Fig. 2D and E, LE135 and HX531 also offset the inhibitory effect of ATRA on the signal intensities for ssDNA and active caspase-3 in the slices treated with OGD/Rep. Thus, the intensities for ssDNA and active caspase-3 were negatively associated with the abundance of NeuN.

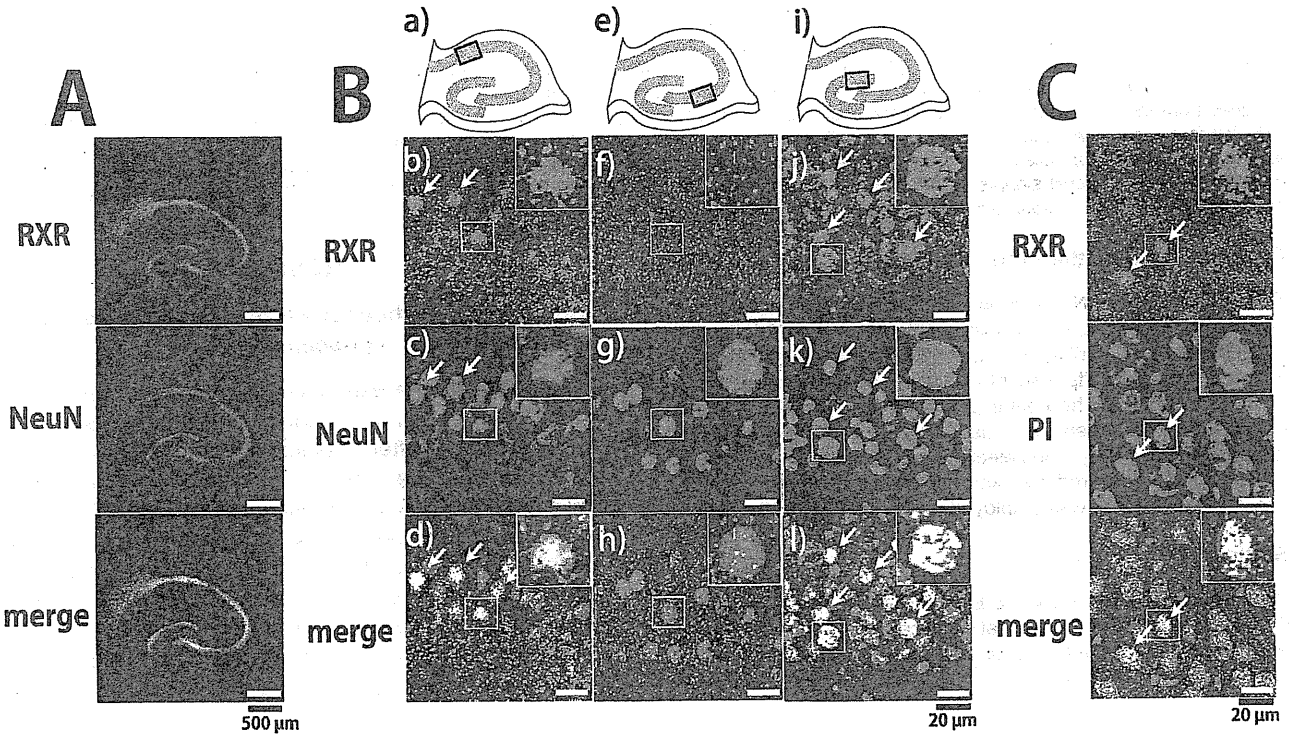

Fig. 4. Subregional expression pattern of RXR in the hippocampus. (A) Immunostaining for RXR showed neuronal cell layer-like pattern in CA1 to CA3 and in DG (upper panel). The signals for RXR were colocalized with those for NeuN (lower panel). Scale bar=500 μm. (B) Differences in the expression pattern of RXR between subregions of hippocampus. Images in b–d were obtained from the CA1 region indicated by the square in a. The signals for RXR appeared in diffusion-forms in CA1 (b; arrows). The signals for NeuN signals (c) were colocalized with those for RXR (d). Images of f–h were obtained from the CA3 region indicated by the square in e. In contrast to CA1, the RXR signals were barely detectable in CA3 (f), though they were colocalized with the NeuN signals (g, h). Images in j–l were obtained from the DG region indicated by the square in i. The RXR signals in DG were colocalized with those for NeuN (j–l, arrows). RXR-positive neurons were more frequent in DG, compared with CA1. (C) RXRs exist in the nucleus. RXRs in CA1 were colocalized with PI signals (arrows). The insets show highly magnified images of the square-selected region. Scale bar=20 μm.

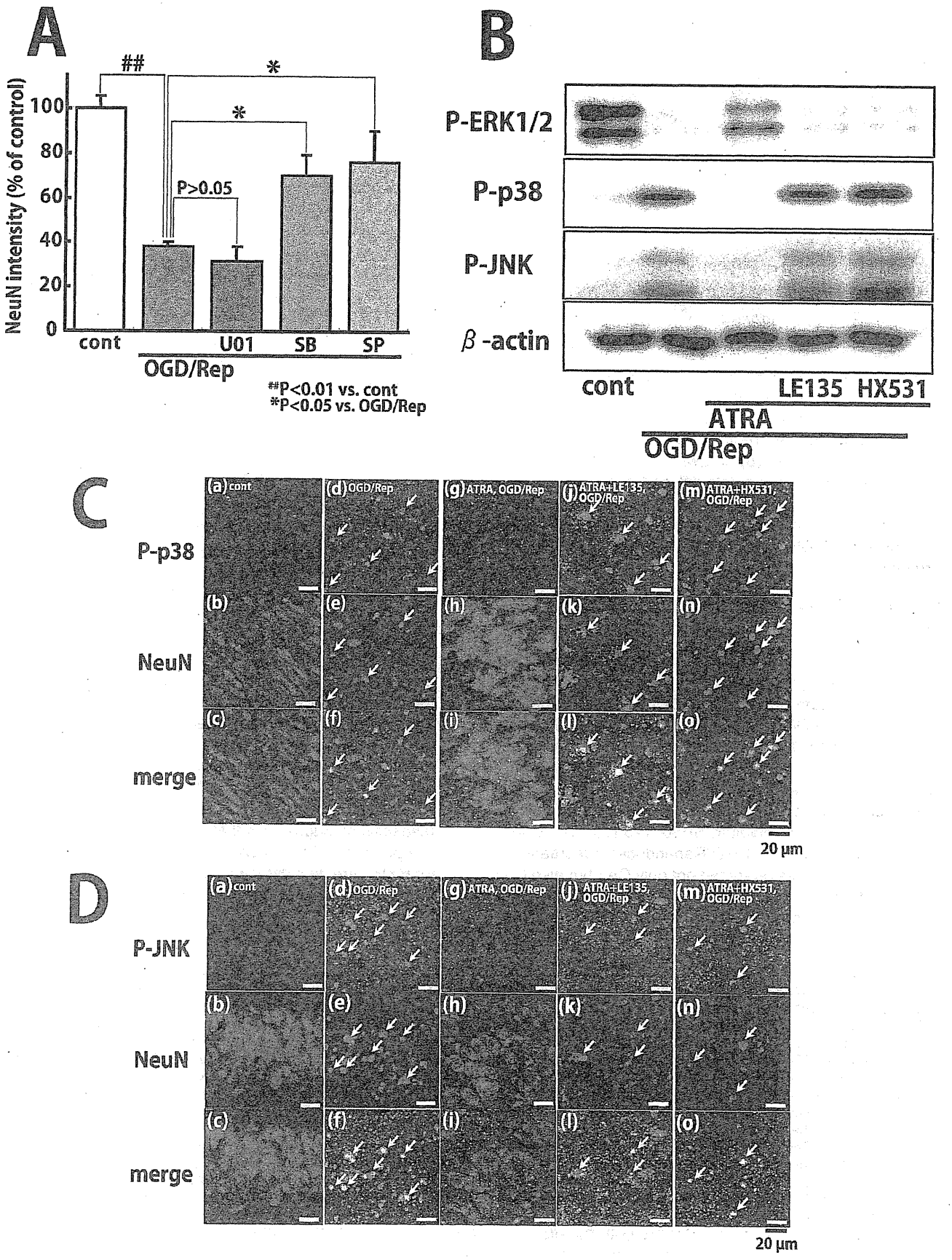

Fig. 5. (*Caption overleaf*)

Subregional differences of RAR and RXR expression in the hippocampus

To determine the expression of RAR and RXR in the hippocampus, we performed immunohistochemical analyses of the tissue slices using specific antibodies for RAR and RXR. In hippocampal slices fixed right after dissection from rat hippocampus, RAR was expressed in CA1 to CA3 and DG (Fig. 3A) and was colocalized with NeuN. Misner et al. (2001) have shown RA signaling activity in CA1, CA2, CA3 and DG of hippocampus, consistent with our results. RXR was also expressed in CA1 to CA3 and DG, and colocalized with NeuN (Fig. 4A). At higher magnification, subregional differences of RAR and RXR expression were observed in the hippocampus (Figs. 3 and 4). Diffused signals of RAR were observed in DG (Fig. 3B (j), arrows), and parts of them were in ring-formation (Fig. 3B(j), arrowheads). Almost all of RAR in square-selected region of CA3 (Fig. 3B(e)) were in ring-formation (Fig. 3B(f), arrows), and parts of them were in diffusion-forms (Fig. 3B(f), arrowheads). In the CA1 region, almost all of RARs were in ring-formation (Fig. 3B (b), arrows). The RXR signals from cells in CA1 and DG were dots diffused in the nucleus (Fig. 4B, arrows) and those in CA3 subregions were barely detectable (Fig. 4B, center). RAR and RXR were also colocalized with DNA-binding dye PI (Fig. 3C and Fig. 4C, arrows).

Inhibitory effect of ATRA on OGD/Rep-induced MAPK activation

As MAPKs have been associated with various physiological and pathological events including ischemia-induced neuronal cell death (Xia et al., 1995), we examined the role of MAPKs in the OGD/Rep-induced neuronal death, using specific inhibitors for subgroups of MAPK signaling. As shown in Fig. 5A, MEK1/2 (ERK kinase) inhibitor U0126 (10 μM) had no effect on the decrease in NeuN after OGD/Rep. In contrast, both a p38 inhibitor, SB203580 (20 μM), and a JNK inhibitor, SP600125 (20 μM), significantly prevented the OGD/Rep-induced decrease in NeuN. Both inhibitors protected not only CA1 but also CA3 neurons (data not shown), suggesting that the two kinases were activated in both subregions after OGD/Rep. Western blot analyses revealed that the OGD/Rep led to a decrease in P-ERK1/2 and increases in P-p38 and P-JNK. Pretreatment with ATRA (100 nM) prevented these changes in phosphorylated MAPKs, which were abolished in the presence of LE135 (1 μM) or HX531 (1 μM). To confirm whether OGD/Rep increased P-p38 and P-JNK in neuronal cells, immunohistochemical analyses were performed. In controls, signals for P-p38 and P-JNK were hardly detectable (Fig. 5C(a–c), 5D(a–c)), but seemed to exist in the cytoplasmic region. OGD/Rep enhanced the signals for both P-p38 and P-JNK, which were colocalized with the signals for NeuN (Fig. 5C(d–f), 5D(d–f), arrows). The NeuN signals were shrunk in OGD/Rep-treated slices, compared with the controls (Fig. 5C(b) and (e), 5D(b) and (e)). Pretreatment with ATRA (100 nM, 24 h) decreased the P-p38 and P-JNK signals, which were faintly detected around the NeuN signals (Fig. 5C(g–i) and 5D(g–i)). The shrinkage of the NeuN signal was also prevented by ATRA treatment. LE135 (1 μM) and HX531 (1 μM) inhibited the effects of ATRA (Fig. 5C(j–o), arrows and Fig. 5D(j–o), arrows).

DISCUSSION

In the present study, we demonstrated that ATRA induces a protective effect against OGD/Rep-induced damage in neurons from cultured hippocampal slices. The effect of ATRA was inhibited not only by a RAR antagonist but also by a RXR antagonist, indicating that ATRA-induced protection was mediated by RAR/RXR heterodimer. Selective RXR agonists and antagonists are known to synergistically enhance and inhibit activity of RAR in RAR/RXR heterodimers, respectively, and the opposite is observed in the case of RAR agonists and antagonists (Ebisawa et al., 1999). In the CA3 region, where ATRA had no neuroprotective activity, both a ring-formed and diffusion-formed distribution of RARs in the nucleus was found. However, a ring-formed as well as a diffuse-formed distribution of RARs mediated neuroprotection of ATRA in CA1 and DG, respectively, suggesting that the neuroprotective effect is independent of the pattern of RAR distribution. The signals for RXR were dots diffused in the nucleus. Unlike RAR that forms a heterodimer with RXR, RXR forms not only homo/heterodimers but also a homotetramer (Kersten et al.,

Fig. 5. The role of MAPK activation in the OGD/Rep-induced cell death of hippocampal neurons. (A) The effect of MAPK inhibitors on the OGD/Rep-induced decrease in NeuN. MEK1/2 inhibitor U0126 (10 μM) had no effect on the decrease in NeuN by OGD/Rep. Both p38 inhibitor, SB203580 (20 μM), and JNK inhibitor, SP600125 (20 μM), significantly inhibited the OGD/Rep-induced decrease in NeuN. All the MAPK inhibitors were added to the culture medium during Rep. Values were expressed as means±S.E.M. of the fluorescent signal intensities for NeuN (n=3). (B) The effect of ATRA on OGD/Rep-induced changes in the levels of phosphorylated MAPKs. P-ERK1/2 was decreased by OGD/Rep, which was prevented by ATRA (100 nM, 24 h). The effect of ATRA on P-ERK1/2 was inhibited by LE135 (1 μM) or HX531 (1 μM). The increases in P-p38 and P-JNK, induced by OGD/Rep, were prevented by ATRA (100 nM, 24 h). The effects of ATRA on P-p38 and P-JNK levels were inhibited by LE135 (1 μM) or HX531 (1 μM). (C) Immunohistochemical analyses of p38 activation by OGD/Rep. In the controls, P-p38 was hardly detectable (a–c). The OGD/Rep led to an increase in the signals for P-p38 (d), as well as a shrinkage of the signals for NeuN (e; arrows). The P-p38 signals were colocalized with those for NeuN (f; arrows). The OGD/Rep resulted in the shrinkage of the NeuN signals (e; arrows). ATRA (100 nM, 24 h) prevented the increase in the P-p38 signals (g) and the shrinkage of the NeuN signals (h) after OGD/Rep. The effects of ATRA were inhibited by LE135 (1 μM) (j–l) or HX531 (1 μM) (m–o). The P-p38 signals were colocalized with signals for NeuN (l, o; arrows). (D) Immunohistochemical analysis of JNK activation by OGD/Rep. In the controls, P-JNK was hardly detectable in the NeuN-positive regions (a–c). In the areas of surrounding the NeuN signals, P-JNK signals were sparsely observed. P-JNK signals were significantly increased by OGD/Rep, which were colocalized with those for NeuN (d–f; arrows). ATRA (100 nM, 24 h) prevented the increase in P-JNK by OGD/Rep (g–i). The effect of ATRA was inhibited by LE135 (1 μM) (j–l) or HX531 (1 μM) (m–o). The P-JNK signals were colocalized with those for NeuN (arrows). ATRA (100 nM) was added to the slices 24 h before OGD and during Rep. LE135 (1 μM) and HX531 (1 μM) were added to the culture medium 30 min before ATRA treatment. Scale bar=20 μm.

1995). Such differences in the multimeric structure may lead to the difference in the pattern of receptor distribution. In contrast to RAR, RXR was barely expressed in the CA3 region. Therefore, the lack of the synergistic effect of RXR in CA3 may explain the subregional difference in the cytoprotective effect of ATRA. In addition, 9-*cis* RA, an agonist for both RAR and RXR, also showed no protective effect on CA3, suggesting a deficiency in the receptor heterodimer activity in this region. Furthermore, degradation rates of RAs in CA3 may also contribute to their subregion-selective effects, because the RA degrading enzyme CYP26B1 is known to be strongly expressed in the CA3 region (Abu-Abed et al., 2002). According to the report of Misner et al. (2001), endogenous retinoid signaling is active throughout the hippocampus (i.e. CA1–CA3 and DG). However, they also showed that the retinoid signaling activity is the most potent in the DG, followed by CA1 and hilus, and relatively low in CA3, which is consistent with our results.

We found that ATRA potently inhibited the increases in activated forms of p38 (P-p38) and JNK (P-JNK) after OGD/Rep, which was offset by RAR or RXR inhibitors. In addition, inhibition of JNK and p38 activity by their specific inhibitors prevented neuronal damage by OGD/Rep, indicating the death-promoting functions of JNK and p38 in OGD/Rep. These findings suggest that ATRA, acting through RAR/RXR, protects hippocampal neurons from OGD/Rep stress, at least partly, by preventing the activation of JNK and p38. ATRA is known to increase the expression of mitogen-activated protein kinase phosphatase-1 (MKP-1), protecting mesangial cells from H_2O_2-induced cell death by dephosphorylation and inactivation of JNK and p38 (Konta et al., 2001). Recently, MKP-1 was found to primarily dephosphorylate JNK and p38, but not ERK1/2 (Wu and Bennett, 2005). Therefore, upregulation of MKP-1 is one possible mechanism in the neuroprotective effects of ATRA, observed in the present study. Recent studies have shown that molecules generally called "nuclear receptors" (i.e. RXR, TR and steroid hormone receptors) elicit non-genomic effects in response to their agonists (Hiroi et al., 2006; Wehling and Losel, 2006; Moraes et al., 2007). Additionally, ATRA is known to phosphorylate neuronal ERK in a nongenomic manner (Canon et al., 2004), which is consistent with its inhibitory effect on OGD/Rep-mediated ERK dephosphorylation. In the present study, selective RAR or RXR antagonists inhibited the neuroprotection by ATRA. Furthermore, ATRA applied after OGD was also neuroprotective. Therefore, it is also possible that ATRA protected hippocampal slices from OGD/Rep-induced cell injuries via the non-genomic action of RAR or RXR.

In contrast to JNK and p38, ERK1/2 mediates the pro-survival functions in staurosporine-treated neurons (Zhu et al., 2002). It has been suggested that BDNF is the mediator for the pro-survival effect of ERK1/2 (Han and Holtzman, 2000). ATRA is known to upregulate Trk B, the receptor for BDNF, NT-3 and NT-4/5, facilitating BDNF signaling (Kaplan et al., 1993; Kobayashi et al., 1994). Although the inhibition of endogenous ERK1/2 activity by a MEK inhibitor did not facilitate cell death by OGD/Rep, ATRA inhibited an OGD/Rep-induced decrease in P-ERK1/2. Therefore, it is still possible that P-ERK1/2 also contributes to the neuroprotection of ATRA under OGD/Rep.

CONCLUSION

In conclusion, our results suggest that ATRA has a protective effect on hippocampal neurons against OGD/Rep-induced damages, by inactivating JNK and p38 via RAR/RXR heterodimers. As ATRA is a lipophilic molecule, orally applied ATRA can easily reach the CNS thorough blood–brain barrier (Crandall et al., 2004). Although relatively high concentrations of ATRA (10–100 nM) were necessary for the neuroprotection in our ex vivo model, they are achievable by an oral administration of ATRA not only in rats but also in humans in a clinical setting (Saadeddin et al., 2004; Muindi et al., 1992). Therefore, our findings provide new insights into clinical applications of ATRA for the treatment of CNS diseases such as stroke.

Acknowledgments—We thank Dr. Koichi Shudo for the gracious gift of LE135 and HX531, and we thank Tomoko Obama for technical assistance. We are grateful to Dr. Helen Kiriazis for critical reading of the manuscript. This study was partly supported by grants from National Institute of Biomedical Innovation (MF-16), from the Uehara Memorial Foundation, and from the Ministry of Health, Labor and Welfare of Japan, and grants-in-aid for Scientific Research (B) and (C), for Young Scientists (A) and on Priority Areas (A) from the Ministry of Education, Science, Sports and Culture of Japan.

REFERENCES

Abu-Abed S, MacLean G, Fraulob V, Chambon P, Petkovich M, Dolle P (2002) Differential expression of the retinoic acid-metabolizing enzymes CYP26A1 and CYP26B1 during murine organogenesis. Mech Dev 110:173–177.

Ahlemeyer B, Krieglstein J (1998) Retinoic acid reduces staurosporine-induced apoptotic damage in chick embryonic neurons by suppressing reactive oxygen species production. Neurosci Lett 246:93–96.

Behrens A, Sibilia M, Wagner EF (1999) Amino-terminal phosphorylation of c-Jun regulates stress-induced apoptosis and cellular proliferation. Nat Genet 21:326–329.

Boulton TG, Nye SH, Robbins DJ, Ip NY, Radziejewska E, Morgenbesser SD, DePinho RA, Panayotatos N, Cobb MH, Yancopoulos GD (1991) ERKs: a family of protein-serine/threonine kinases that are activated and tyrosine phosphorylated in response to insulin and NGF. Cell 65:663–675.

Canon E, Cosgaya JM, Scsucova S, Aranda A (2004) Rapid effects of retinoic acid on CREB and ERK phosphorylation in neuronal cells. Mol Biol Cell 15:5583–5592.

Chambon P (1994) The retinoid signaling pathway: molecular and genetic analyses. Semin Cell Biol 5:115–125.

Chambon P (1996) A decade of molecular biology of retinoic acid receptors. FASEB J 10:940–954.

Chen J, Nagayama T, Jin K, Stetler RA, Zhu RL, Graham SH, Simon RP (1998) Induction of caspase-3-like protease may mediate delayed neuronal death in the hippocampus after transient cerebral ischemia. J Neurosci 18:4914–4928.

Chiang MY, Misner D, Kempermann G, Schikorski T, Giguere V, Sucov HM, Gage FH, Stevens CF, Evans RM (1998) An essential